THE EXTRATROPICAL 40-DAY OSCILLATION IN THE UCLA GENERAL CIRCULATION MODEL
PART I: ATMOSPHERIC ANGULAR MOMENTUM

by

S. L. Marcus[1,2,*], M. Ghil[2], and J. O. Dickey[1]

[1]Space Geodetic Science and Applications Group
Jet Propulsion Laboratory
California Institute of Technology
Pasadena, California 91109-8099

[2]Climate Dynamics Center, Department of Atmospheric Sciences
and Institute of Geophysics and Planetary Physics,
University of California, Los Angeles

* Present address: Jet Propulsion Laboratory,
Pasadena, CA

Abstract

Fluctuations in atmospheric angular momentum (AAM) are examined in a three-year simulation of the perpetual-January climate, performed with of a version of the UCLA general circulation model which contains no tropical, Madden-Julian oscillation (MJO). In addition, the results of three shorter experiments with no topography are analyzed. The three-year, standard-topography run contains no significant intraseasonal AAM periodicity in the tropics, consistent with the lack of the MJO, but produces a robust, 42-day AAM oscillation in the northern hemisphere (NH) extratropics. The model tropics undergoes a barotropic, zonally-symmetric oscillation, driven by an exchange of mass with the NH extratropics. No intraseasonal periodicity is found in the average tropical latent heating field, indicating that the model oscillation is dynamically- rather than thermodynamically-driven. The no-mountain runs fail to produce an intraseasonal AAM oscillation, consistent with an topographic origin for the NH extratropical oscillation in the standard model. The spatial pattern.. of the oscillation in the 500 mb height field, and the relationship of the extratropical oscillation to intraseasonal variations in the tropics, are discussed in Part II of this study,

1. Introduction

a Background and motivation

Since the pioneering work of Madden and Julian (1971, 1972; MJ hereafter), two distinct types of oscillations with periods between one and two months have been documented in the Earth-atmosphere system, The eastward-propagating, tropical systems of anomalous convective activity first described by MJ are dominated by a baroclinic, zonal wavenumber-one structure (e.g. Knutson and Weickmann 1987). An oscillation on a similar time scale, observed in troth the axial component of atmospheric angular momentum (AAM) and in the rotation rate of the solid Earth (e.g. Langley et al. 1981; Dickey et al. 1991), has a very large barotropic, wavenumber-zero component. Due to the rough coincidence in frequency, it is reasonable to speculate that these two oscillations are linked (Anderson and Rosen 1983; Madden 1987; Madden 1988; Weickmann et al. 1992), although the precise physical connections have yet to be established.

The selection mechanism for the preferred 40-50 day period of these oscillations is also open to question, For the MJ oscillation, the observed near-periodicity has been assumed to result from the transit time of eastward-propagating, connectively-driven waves around the equator (Lorenc 1984; Knutson and Weickmann 1987; Lau and Peng 1987), or from a combination of such tropical waves and of extratropical Rossby waves traveling along an approximate great circle route involving legs in the northern (Lau and Phillips 1986; Hsu et al. 1990) or southern (Gao and Stanford 1988) hemisphere extratropics. If the AAM oscillation is generated by rectification of the MJ wave, its period would also be determined by a propagation time scale.

Recent studies have shown, however, that oscillations with similar periods can arise in the extratropical atmosphere from nonlinear instabilities in the presence

of constant thermal-wind forcing. Using a simple, equivalent-barotropic model of flow over idealized northern hemisphere topography, Legras and Ghil (1985) found that oscillations with a period near 40 model days arise by Hopf bifurcation from a blocked stationary state as the steadily-forced, zonally-symmetric thermal wind is increased beyond a critical value. The mechanism of this oscillation, and its relationship to the AAM oscillation, were further discussed by Ghil (1987), by Ghil and Childress (1987, pp. 164-201), and by Jin and Ghil (1990). This oscillatory instability of the blocked flow in the simple model is related to changes in the intensity and meridional position of the jet, as well as in the amplitude and longitudinal phase of its meanders with respect to the fixed topography. Similar oscillations have subsequently been found in dynamical models with higher horizontal (Tribbia and Ghil 1990; Strong et al. 1993) and vertical (Keppenne 1989) resolution. To determine whether the nonlinear oscillations found in this simple class of model can serve as the prototype for 40-S0 day variability as observed in the atmosphere, we assess the presence of similar oscillations in a much more complete model of the atmosphere, namely a general circulation model (GCM).

b. Plan of the investigation

In Part I of this study, we examine AAM fluctuations arising in a three-year perpetual-January simulation of the global atmosphere, performed using a version of the UCLA GCM which suppresses the MJ oscillation. The absence of seasonal forcing and of MJ oscillations in the model tropics enable us to isolate a nonlinear, intraseasonal oscillation in AAM arising in the northern hemisphere (NH) extratropics of the model. Three shorter experiments utilizing distinct versions of the UCLA GCM with all surface elevations set to zero are also used in the analysis. In Section 2, the basic features of the UCLA GCM and of the perpetual-January simulations are described, In Section 3, the wavenumber-zero component of the

oscillation is investigated by analyzing the behavior of the model's AAM, both globally and by latitude bands. A summary and discussion of the findings are given in Section 4. Observational evidence for the existence of a separate extratropical oscillation in AAM, distinct from the tropical MJ oscillation, was discussed in an earlier study (Dickey et al. 1991). The spatial characteristics of the UCLA GCM oscillation at 500 mb in the NH extratropics, and teleconnections with the 500 mb height field and convective activity in the tropics, are discussed in Part 11 of this study.

2 Description of the model and the simulations

a. Model description

Only a brief description of the model is given here; a complete documentation is provided by Suarez et al. (1983), and the references contained therein. The UCLA GCM is a comprehensive model for the evolution in time of the dynamic and thermodynamic fields representing the global atmosphere, Its prognostic variables are the horizontal velocity, the potential temperature, the water vapor mixing ratio, the ozone mixing ratio, the surface pressure, the planetary boundary layer (PBL) depth, and the ground temperature. In the vertical, the model is based on a modified sigma-coordinate system for which the lower boundary, the PBL top, and isobaric surfaces above a prescribed pressure level (100 mb) are coordinate surfaces. The top of the model atmosphere is assumed to be a material surface, The vertical finite-differencing used above the PBL is that described by Arakawa and Suarez (1983). It guarantees conservation of the global mass integrals of potential temperature and total potential plus kinetic energy under frictionless adiabatic processes.

The equations are horizontally discretized using a staggered latitude-longitude grid, The scheme for the horizontal advection terms in the momentum

equation is baaed on the potential-enstrophy conserving scheme presented by Arakawa and Lamb (1981), modified to give fourth-order accuracy for the advection of potential vorticity. The horizontal advection scheme used for the potential temperature is also of fourth order and conserves the global mass integral of its square. All other terms in the continuity equation, the pressure gradient force, and the definition of absolute vorticity use differencing of second-order accuracy. The model and its ability to simulate the observed climate are discussed further by Mechoso et al. (1987).

b. General features of the simulations

The GCM's standard low-resolution spatial grid was used for this study. It has a horizontal mesh of 4 degrees latitude by 5 degrees longitude, 9 vertical layers, with the top at 51.8 mb, and realistic distributions of surface topography and sea ice, at this resolution. The model was started from the observed data for 15 November 1982, and was run with seasonally-varying solar declination and climatological sea-surface temperature to a simulated time of 15 January 1983. At this point the solar declination and sea-surface temperatures were held fixed, and the model was run for 1120 days in a perpetual-January mode.

In order to test the influence of topography on the model's intraseasonal variability, three shorter perpetual-January experiments, starting from the same initial state as the standard three-year run, were performed with all surface elevations set to zero (see Table 1). The first of these experiments used the exact same numerical code and boundary conditions as the standard run, and continued for 300 days. The second experiment, lasting 380 days, used sea-surface temperatures observed during January 1983, at the height of an intense El Niño/Southern Oscillation (ENSO) event, For the third experiment, lasting 350 days, a new

formulation for the long-wave radiation scheme was implemented. The results of the no-mountain runs are discussed in Section 3f.

Even though the model generates its own radiatively-interactive cloud cover and snow fields, little climatic drift is evident during the course of the experiments. Profiles of the zonally-averaged surface temperature and of the w-weighted zonal wind for the northern hemisphere are given in Figs. la and lb, respectively, for the standard-topography experiment; averages for the first, second, and third years of the run (defined to be days 1-370, 371-740, and 741-1120) are shown by the solid, dashed, and dotted lines, respectively. No secular trend can be seen in either the thermal gradient driving the model's midlatitude circulation, or in the resulting basic state of the model's angular momentum distribution.

3. Angular momentum fluctuations

a. Introduction

The axial component of atmospheric angular momentum in an inertial reference frame is given by

2a

$$M_a = \int_0^{2\pi} \int_{-\pi/2}^{\pi/2} \int_{r_s(\phi,\lambda)}^{\infty} \rho v r^3 \cos^2\phi \, dr \, d\phi \, d\lambda \qquad (1)$$

where λ is the longitude,. # the latitude, r is the distance to the center of the Earth, and v the east-west wind velocity. Writing v in terms of the Earth's angular velocity Ω and the relative zonal wind velocity u as

$$v = r\Omega \cos\phi + u \qquad , \qquad (2)$$

the change in angular momentum from a state of rest for a hydrostatic atmosphere occupying a thin spherical shell can be approximated as

$$\delta M_a = \frac{a^3}{g}\int_0^{2\pi}\int_{-\pi/2}^{\pi/2}\int_0^{p_s(\phi,\lambda)} u\cos^2\phi\, dp\, d\phi\, d\lambda + \frac{\Omega a^4}{g}\int_0^{2\pi}\int_{-\pi/2}^{\pi/2}\cos^3\phi\,\delta p_s\, d\phi\, d\lambda \quad , \qquad (3)$$

where a is the mean radius of the Earth, δp_S the deviation of the surface pressure from a standard value, and the gravitational acceleration g is assumed to be constant over the depth of the atmosphere.

The two terms on the right-hand side of Eq. (3) represent AAM fluctuations caused by variations in relative zonal velocity and the atmosphere's moment of inertia, respectively, and are referred to as the wind and pressure terms (Barnes et al, 1983). Note that while the wind term can be readily decomposed by latitude, the pressure term, due to the constraint of global mass conservation, is best described by the integral formulation given in Eq. (3). Observational evidence shows that the wind term dominates AAM variations on intraseasonal time scales (for a review see Hide and Dickey 1991). In addition, the rotational response of the Earth to variations in atmospheric mass distribution is attenuated by the presence of the oceans, which act to partially offset surface pressure changes through the "inverted barometer" effect (Lambeck 1980). For these reasons, most studies of atmospheric excitation of LOD fluctuations have concentrated on the wind term and, unless otherwise noted, subsequent references to model AAM fluctuations are given for the wind term only. The role of the pressure term in the model's intraseasonal oscillation will be discussed in Section 3g.

On time scales of a few years or less, changes in the Earth's rotation rate, and therefore in the length-of-day (LOD), are primarily forced by exchanges of angular momentum with the atmosphere (Eubanks et al. 1985). Various studies (e.g. Rosen and Salstein 1983; Eubanks et al. 1985; Dickey et al, 1986) have shown the excellent match achieved between estimates of AAM obtained from the

assimilation of atmospheric data into numerical weather prediction models, on the one hand, and LOD estimates from modern geodetic methods, on the other, For purposes of comparison with geodetic data (cf. Dickey et al. 1991), AAM fluctuations are given in units of LOD variation, obtained by the formula

$$LOD = \frac{LOD_0}{\Omega} \frac{\delta M_a}{C} \tag{4}$$

where LOD_0 is the standard length of the day, and C is the combined moment of inertia of the Earth's crust and mantle. While exchanges of angular momentum between the liquid core and the solid Earth can occur on decadal time scales, the core is not believed to participate noticeably in seasonal or sub-seasonal rotational variations (Hide 1977; Hide and Dickey 1991).

The deviation of the global AAM from its time-mean value, plotted in LOD units, is shown for the standard-topography run in Fig. 2 (upper panel). The lower three panels in Fig. 2 show AAM anomalies computed separately for the latitude belts 90N-20N, 20N-20S, and 20S-90S, hereafter referred to as the northern hemisphere (NH) extratropics, tropics, and southern hemisphere (SH) extratropics, respectively. The latitudes 20S and 20N, rather than 30S and 30N, were chosen to give three regions of approximately equal area, and to ensure that the subtropical jets are included consistently in the extratropical regions, rather than the tropical one.

In spite of the absence of seasonal forcing, variation of the AAM series on a variety of time scales is evident, The root-mean-square (rms) deviation of the simulated global AAM is 0,078 ms, compared to a value of 0.170 ms for seasonal residuals from modem geodetic LOD measurements, as well as from NMC AAM data (Eubanks et al. 1985). Thus the model captures about half of the intraseasonal variability present in the real atmosphere. The reduced amplitude of the simulated

intraseasonal variability is probably due to the absence of the MJ oscillation from this model version.

The root-mean square (rms) deviations of the AAM series for the NH extratropics, tropics, and SH extratropics are 0.046ms, 0.064ms, and 0.022ms, respectively. In spite of the absence of MJ oscillations the tropical belt has the largest AAM variance, due to its greater mean distance from the rotation axis. The AAM series for the NH extratropics has about half the power of the tropical series, while the SH extratropics, in perpetual summer, has much less AAM variability than the other two regions. The slight upward trend visible in the NH AAM series appears to be related to very low-frequency variability (cf. James and James 1992), and is absent in either the first or last three-quarters of the run considered separately.

b. Autocorrelations

In order to search for periodicities in the model output, we adopt the "null hypothesis" of a first-order autoregressive (AR 1) process, for which the autocorrelation function (ACF) has the form

$$r(t) = \exp(-t/\tau),$$

where t is the lag and τ is the decorrelation time for the process. Since we are interested in the behavior of the model's AAM on time scales of weeks rather days, τ was taken to be the time at which the sample ACF decays to l/e, in lieu of an estimation baaed on the value at a one-day lag (cf. Madden 1976). The sample ACFS for the model's global AAM, and those for the NH extratropics, tropics, and SH extratropics, are shown in Fig. 3.

The decorrelation time for the tropical AAM series is almost 11 days, while the SH extratropics has a decorrelation time of about eight days and the NH extratropics only six days. The low decorrelation time for the latter region presumably reflects the activity of baroclinic disturbances, which have about the

same time scale (e.g. Legras and Ghil 1985). The weaker synoptic-sale activity in the SH extratropics (experiencing perpetual summer) and in the deep tropics is reflected in the progressively longer AAM decorrelation times for these regions. Due to its greater distance from the rotation axis, the tropical region dominates the overall AAM budget, leading to a global decorrelation time (10.6 days) only slightly less than that for the tropics itself.

The ACF estimate for the global AAM, after reaching value-s near zero at a lag of 31 days, shows a clear secondary maximum at a period of 41 days. For lags which are long compared to the decorrelation time but short compared to the length of the record, the variance of the sample ACF for an AR 1 process is approximately equal to the ratio of the decorrelation time to the total record length (Jenkins and Watts 1968, Ch. 5). While the height of the secondary ACF maximum seen for the global AAM at 41 days is not statistically significant by this criterion, further evidence will show that it represents a real 40-50 day AAM oscillation in the perpetual-January climate of the GCM.

The ACF estimate for the NH extratropics reaches a minimum at a lag of 26 days, followed by a secondary maximum of 0.265 at a lag of 40 days. This exceeds the standard deviation of the NH ACF estimator by more than a factor of three, and represents a highly significant departure from an AR1 process at this lag. While the maximum in the ACF estimate at a lag of about 80 days is not statistically significant, it is consistent with the presence of harmonics in a nonlinear oscillator with a dominant period of 40 days.

The ACF estimate for AAM in the tropical region shows no secondary maximum in the intraseasonal band, consistent with the lack of an MJ oscillation in this version of the model. The minimum value reached at a lag of 52 days is statistically significant, however, and, along with the secondary maximum (not significant) at a lag of 93 days, indicates the presence of longer-period oscillations in

the model tropics. The ACF estimate for AAM in the SH extratropics, characterized by the lesser role of topography, shows no significant departure from that for an AR1 process.

c. *Power spectra*

The spectral analysis technique used here follows that of Eubanks et al, (1985). After tapering the first and last 10% of the data with a cosine bell function, a fast Fourier transform is applied, and the resulting periodogram is smoothed with a moving average in frequency. Approximate confidence intervals for the smoothed spectra were calculated using the method of Brillinger (1975, Sect. 5.7), and are plotted as deviations from the appropriate AR1 model on the subsequent spectra, whenever the spectrum of the latter is shown.

Fig. 4 shows AAM power spectra for the model's global domain, as well as for the NH extratropics and tropics; the AAM power for the SH extratropics is quite small and is not shown. For consistency with the parallel observational study of Dickey et al. (1991), the intraseasonal band considered here will be defined as that corresponding to oscillations with periods between 36 and 60 days. Higher-frequency AAM oscillations, with periods between 16 and 24 days, were also found in the GCM results as well as in the observational study.

For the global AAM, the highest spectral density over the 10-100 day range shown in the figure occurs at a period of 46 days, where the power exceeds the 95% confidence limit for deviations from an equivalent AR1 process. This period coincides roughly with the period of the secondary maximum seen in the ACF estimate in Fig, 3, confirming the presence of a significant intraseasonal oscillation in the model's global angular momentum budget. Enhanced AAM power is also evident in the 16-24 day band, with a sharp peak centered at a period of 21 days. A westward-traveling wave with about this frequency has been observed in NH data at

500 mb and at other levels, especially at high latitudes, by Branstator (1987) and Kushnir (1987). Ghil and Mo (1991a,b) have also studied an oscillation in this frequency range using NH 700 mb data, tropical OLR data and SH 500 mb data,

The spectral estimates for the NH extratropics, like those for the global AAM, emerge significantly above the ARl background in both the 36-60 day and the 16-24 day bands. Unlike the global spectrum, however, the lower-frequency (42-day) peak for the NH extratropics is more statistically significant than the higher-frequency (21-day) peak. The 42-day peak has the largest power spectral density in the NH extratropics for periods up to 150 days (not shown), and corresponds closely in frequency to the ACF maximum seen in Fig, 3. These results demonstrate the existence of a robust AAM oscillation with a period near 40 days in the model's NH extratropics.

Due to its larger mean distance from the rotation axis, the background power level for the spectrum of AAM from the tropical region is considerably higher than that for the NH extratropics. The largest spectral peak in the 36-60 day band occurs at 46 days, coincident in frequency with the global AAM peak. The spectral power of the entire 36-60 day band is depressed relative to a red-noise process, however, consistent with the lack of an intraseasonal signal in the ACF estimate for the tropical AAM (Fig. 3). These findings reflect the absence of a vigorous MJ oscillation in this version of the GCM, a fact which has been corroborated by other UCLA investigators (A. Arakawa, personal communication); another version of this GCM, implemented at the Meteorological Research Institute in Japan, does exhibit tropical, MJ-type oscillations (Tokioka et al. 1988).

As for the NH extratropics, the AAM spectrum for the tropics shows a modest peak at 21 days (see also Ghil and Mo 1991a); apparently, coherent addition of the signals in these two regions produces the high] y-significant 21 da y peak seen in the global AAM spectrum. At other periods, however, the tropical AAM

spectrum is statistically indistinguishable from that of a red-noise process. The relationship between AAM variations in the model tropics and NH extratropics is illustrated in Fig, 5, which shows the power spectra for these two regions on a linear scale; the effects of the differing mean axial distance on AAM variations from the two regions has been removed, so that the continuous, red-noise background power levels characterizing the two spectra are about equal. The NH 42day peak stands out clearly against this common red-noise background, while the 46-day peak in the tropics disappears into the background.

d. Interactions between regions

Fig. 6 shows estimates of the cross-correlation between the AAM time series for the NH extratropics and tropics, tropics and SH extratropics, and NH and SH extratropics, respectively. The 2-sigma confidence interval is indicated by the dotted lines for each plot, based upon the decorrelation time for the AAM series given in Section 3 (Jenkins and Watts 1968, Ch. 8). The only cross-correlation significant at the 95% level occurs between AAM in the NH extratropics and the tropics, with the former region leading by six days. Even though the data have not been filtered, a rough periodicity in the cross-correlation is evident, with secondary maxima found at approximate 40-day intervals before and after the maximum correlation. These correlations indicate that the model tropics responds to the intraseasonal variations arising in the NH extratropics. Further aspects of intraseasonal variability in the tropics are discussed in Section 3g.

The cross-correlations obtained between AAM fluctuations in the tropics and SH extratropics, while not statistically significant, suggest an exchange of AAM between these two regions on time scales of 100 days or more. These fluctuations would presumably be masked by seasonal effects in a model which included the annual cycle, and are beyond the scope of this study. The AAM cross-correlations

between the NH and SH extratropics are not statistically significant, and probably represent random fluctuations rather than physical effects.

e. *Interannual variability*

In order to investigate the behavior of the model's intraseasonal oscillation in the time domain, the AAM series were spectrally filtered to retain oscillations with periods between 36 and 60 days. Fourier decomposition was used, with cosine bell tapering applied to the first and last 10% of the transformed series (Eubanks et al. 1985). The resulting band-pass filter has zero phase distortion, with half-power points at 36,7 and 58.0 days. Fig. 7a shows the band-passed AAM time series for the NH extratropics (solid line) and the globe (dashed line). While both oscillations are intermittent, the NH oscillation is in phase with or slightly in advance of the global AAM oscillation during the periods when the latter has a large amplitude, consistent with the NH extratropical origin of the oscillation.

Fig. 7b shows a smoothed envelope of the 36-60 day AAM oscillation in the NH extratropics, obtained by complex demodulation (cf. Dickey et al. 1991). The amplitude of the oscillation undergoes quasi-regular fluctuations, similar to those seen in other nonlinear climate models for certain ranges of the forcing parameter (Ghil and Childress 1987, Chapters 5 and 12). Similar findings are reported by Ghil and Mo (1991a,b) for the 40-50 day and other intraseasonal oscillations in NH, SH, and tropical data sets, by using singular spectrum analysis (SSA: Vautard and Ghil 1989), rather than complex demodulation, In Part II of this study, the ultralow-frequency modulation of the model's AAM oscillation will be related to the dynamics of the NH extratropics, through the leading EOFS of the 500 mb height field.

The robustness of the model's intraseasonal oscillation was investigated by considering the AAM fluctuations separately for each quarter of the run. Fig. 8

shows ACF estimates computed for AAM in the NH extratropics during days 1-280, 281-560, S61-840, and 841-1120 of the standard-topography run, respectively. Each of the separate ACF estimates shows a clear maximum at a period of about 40 days, although the third quarter shows a broad maximum extending to SO days. Due to the shortness of the record lengths involved, none of these ACF estimates were statistically significant, using the methodology of Sections 3b and 3c. However, the ubiquitous presence of an AAM signal in the 36-60 day band for each quarter of the run indicates that the intraseasonal oscillation in the model's NH extratropics, while intermittent, is nevertheless a robust feature of the standard-topography experiment.

f. No-mountain experiments

Three additional perpetual-January experiments with the UCLA GCM, starting from the same initial state as the 1120-day run but with all surface elevations set to zero, were also available for analysis (see Table 1). The first no-mountain experiment used the same code and sea-surface temperature (SST) field as the standard-topography experiment, and was run for 300 days, In the second experiment, the observed SST field for January 1983 was used in place of climatological SSTS. The resulting surface temperature anomaly (Fig. 9a) is characteristic of the warm phase of the ENSO cycle, with maximum positive anomalies located in the eastern equatorial Pacific, For the third experiment, the preliminary version of a new long-wave radiation scheme was employed. The resulting temperature changes are concentrated over the polar land masses, with cooling of up to 20°K found for some locations during NH winter (Fig, 9b).

The three no-mountain experiments, therefore, span a considerable range of boundary variation in both the tropics and extratropics, and constitute a reasonable ensemble in which to test for the presence of intraseasonal oscillations, Fig, 10a shows histories of the zonal velocity in the NH extratropics for the various runs,

weighted by mass and the cosine of the latitude. Following removal of the mountains, each of the no-mountain runs shows a period of damped oscillations lasting for about 40 days. While the curve for the standard-topography case exhibits clearly fluctuations lasting 40-50 days, the fluctuations in the no-mountain experiments appear to be shorter-lived and smaller, following the damping of the initial transients.

Fig. 10b shows ACF estimates calculated for NH extra tropical AAM from each of the experiments; the first 40 days were dropped from the no-mountain experiments to eliminate transients, and only the first 300 days of the standard experiment were considered, in order to have time series of roughly the same length. While the standard case shows a strong maximum near a lag of 40 days, none of the no-mountain experiments shows evidence of periodicity on intraseasonal time scales, By contrast, the ACF estimates for AAM from the tropics from all four experiments are quite similar (not shown), having broad minima near lags of 50 days.

‘he extratropical AAM oscillation in this version of the UCLA GCM appears to depend on the presence of topography, therefore, rather than instabilities linked to specific boundary conditions. As mentioned in the previous sub-section, statistical significance cannot be demonstrated for oscillations in shorter segments (-300 days) of the standard run. The presence of a 40-day maximum in the ACFS for the NH extratropical AAM in four 280-day segments of the standard experiment (Fig, 8), however, in contrast to the lack of a signal at lags of 36-60 days in three different no-mountain runs of similar duration, strongly suggests that the NH extratropical oscillation in the standard model originates from the interaction of the flow field with topography, Further discussion of the mechanism of this oscillation in the UCLA GCM will be given in Part II.

g. Tropical oscillations

No intraseasonal AAM oscillations were found in the model tropics during the standard-topography experiment, consistent with the lack of the MJ oscillation in this version of the model. In Section 3d, however, we saw evidence for a lagged tropical response to intraseasonal variations in the NH extratropics. Power spectra of the area-averaged 500 mb height field (Fig. 1 la) as well as the surface pressure field (Fig. 1 lb) for the tropics, in fact, show pronounced peaks at a slightly longer period (44 days) than that obtained for the NH extratropical AAM oscillation. The nearly identical shape of these two spectra indicates that the 36-60 day tropical oscillation in this version of the UCLA GCM is highly barotropic, in contrast to the baroclinic structure associated with the observed MJ oscillation (e.g. Knutson and Weickmann 1987).

The pronounced spectral peak obtained for the average surface pressure in the tropics, in particular, demonstrates that the total mass content of this region varies in conjunction with the model's 36-60 day oscillation. Fig. 12a shows that this variation takes the form of an exchange with the NHextratropics, for which the intraseasonal fluctuation in mass content (solid line) has a phase nearly opposite to that for the tropics (dashed line). Power spectra for the unfiltered mass content of the two regions (Fig. 12b) show similar structure, with significant peaks occurring at nearly the same frequency as that of the NH extratropical AAM oscillation. In both the time and spectral domains, the intraseasonal mass fluctuation in the NH extratropics is larger than that in the tropics, with the excess variation taken up by the SH extratropics (not shown). The larger amplitude of the mass fluctuation in the NH extratropics indicates that the exchange is driven by the intraseasonal oscillation originating in that region.

The meridional mass exchange depicted in Fig. 12 leads to changes in the planetary angular momentum of the atmosphere, represented by the second integral

in Eq. (3). The concomitant variations in surface pressure lead to compensating deformation of the solid Earth and the oceans, resulting in a considerable attenuation of the LOD changes which would be expected on the basis of a simple exchange of angular momentum between the atmosphere and a rigid Earth (e.g. Hide and Dickey 1991). Since this study focuses on the dynamics of the atmosphere rather than Earth rotation, however, these corrections are not applied to the pressure-term variations discussed below.

The rms amplitude of the 36-60 day tropical mass variation shown in Fig. 12a is 0.41 $*10^{15}$ kg. The excess planetary angular momentum contained by a uniform distribution of this mass over the tropics (20S-20N) as compared to the extratropics (20N-90N) corresponds to an LOD variation of amplitude 0.013 ms (see Marcus 1990, Appendix III for details of this calculation), considerably smaller than the rms LOD fluctuation of 0.032 ms resulting from the 36-60 day global wind variation (Fig. 7a). For periods greater than about 20 days, in fact, the power spectral density in the global wind term dominates that of the pressure term (Fig. 13a). A plot of the global pressure term along with the wind term from the NH extratropics shows that both series have spectral peaks at about the same frequency (Fig. 13b).

Variations in the mass content and relative AAM of the NH extratropics show a high correlation when Fourier-filtered in the 36-60 day band (Fig. 14a), reaching a (negative) maximum value of -0.8 with the AAM, i.e., the wind term leading by two days. Fig. 14b shows that meridional fluctuations in these two quantities are geostrophically related, with the peak of AAM variation occurring at the latitude of the maximum pressure gradient. The pressure fluctuation vanishes at the latitude where the zonal variance of surface topography is the largest, indicating that the pressure oscillation results from an exchange of mass across the main

orography belt in the NH extratropics. The spatial characteristics of the oscillation and their relation to orography are further discussed in Part 11 of this study.

With respect to the 36-60 day oscillation the contributions of the wind and pressure terms to the global AAM (cf. Eq. 3) are nearly in phase, and since the equatorward transfer of w from the extratropics acts to increase the atmosphere's moment of inertia, they add coherently to variations in the global angular momentum budget. The spectrum for the total global AAM (i.e., the sum of the pressure and wind terms) is shown by the solid line in Fig, 15, while the spectrum for the wind term only is plotted with a dashed line. The intraseasonal peak for the total AAM is about 50% larger than that for the wind term only, and occurs at a period (43,5 days) which is statistically indistinguishable from that of the NH extratropical oscillation. By forcing a coherent variation in the planetary angular momentum, therefore, the zonal wind oscillation in the NH extratropics determines the period of maximum power for the total AAM variability of the model in the intraseasonal band. The higher-frequency (21-day) oscillation is also considerably enhanced by the inclusion of the planetary angular momentum.

Tropical oscillations with a large wavenumber-zero component, of the type documented here in the UCLA GCM, have been found at periods of 1-2 months in surface pressure fields by Kousky (1988). He speculated that they might be related to the MJ oscillation, although the tropical fluctuations showed a significant correlation with pressure variations in the extra tropics. In a series of numerical experiments using a zonally-symmetric version of the GLAS GCM with no mountains, Goswami and Shukla (1984) found quasi-periodic variations of the Hadley circulation on time scales of 10-15 and 20-40 days. Since these oscillations were absent in experiments using prescribed, time-constant latent heating, they concluded that the tropical oscillations they obtained were driven by associated, quasi-periodic variations in the zonally-symmetric cumulus heating field.

In order to investigate whether a similar mechanism could be operating in the UCLA GCM, we analyzed the tropical cumulus heating field from the perpetual January run. Fig 16a shows autocorrelation estimates for the zonally-averaged surface pressure and cumulus heating fields in the tropics. While the mass field shows clear evidence of a 40-45 day oscillation, the cumulus heating field is dominated by short-period variability, with no evident intraseasonal Oscillation. The spectral power for the average cumulus heating field, shown in Fig. 16b over the frequency range from 3 to 300 days, is depressed relative to an AR1 process in the 36-60 day band; in the frequency interval from 10 to 100 days, it resembles white noise (Fig. 16c).

Unlike the Goswami-Shukla results, therefore, the zonally-symmetric component of the oscillation found in the UCLA GCM does not appear to be driven by nearly-periodic variations in the latent heating field. Moreover, the period of the pressure-field oscillation in the UCLA GCM (44 days) is closer to that observed for the wavenumber-zero fields in the tropics (--50 days, cf. Dickey et al. 1991); other GCM oscillations driven by latent heating variations have periods in the 20-40 day range (e.g. Hayashi and Sumi 1986; Lau and Lau 1986; Pitcher and Geisler 1987; but see also Hayashi and Golder 1993, who obtain a 40-50 day component). These results suggest that the zonally-symmetric mass fluctuations found in the tropics by Kousky (1988) may result from disturbances originating in the extratropics, as they do in the UCLA GCM.

5. Summary and Discussion

We have examined atmospheric angular momentum (AAM) fluctuations in a three-year (1120-day) perpetual January simulation performed with a version of the UCLA GCM which does not replicate the tropical MJ oscillation; in addition, three

shorter (-300 day) experiments using versions of the UCLA GCM with all surface topography set to zero were examined, In spite of the lack of MJ oscillations in the model tropics, a robust, 40-day oscillation was found to arise in the NH extratropics of the standard-topography run. Evidence of the oscillation was found in each quarter of the standard run considered separately, although the length of these segments (280 days) was too short to demonstrate statistical significance for each of them. By contrast, no evidence for intraseasonal (36-60 day) oscillations was found in the three no-mountain experiments.

The presence of a 40-day oscillation in the standard-topography run is consistent with the theory of Ghil and colleagues (see Ghil [1988] and references therein), who found similar oscillations in barotropic models of flow over idealized NH topography. Simmons et al. (1983) have found linearly unstable modes with periods near 50 days, growing in a barotropic model having the climatological northern hemisphere (NH) winter circulation at 300 mb as a basic state. They suggested that much of the low-frequency variability y of the NH wintertime genera I circulation is associated with disturbances which derive their energy from the basic state through barotropic instability, In their theory, topography contributes only to the maintenance of asymmetries in theclimatological basic state, and is absent from the instability mechanism itself. The absence of oscillations from ail three no-mountain experiments, however, having large differences in boundary conditions and radiative forcing, makes it unlikely that barotropic instability is responsible for the pronounced 40-day oscillations seen in the standard-topography run.

A wavenumber-zero, barotropic oscillation is found to occur in the model tropics, characterized by coherent fluctuations in the average 500 mb height and surface pressure fields. The pressure oscillation results from an exchange of mass with the NH extratropics, driven by the zonal-wind oscillation arising in that region. The resulting fluctuations in planetary angular momentum add coherently to the wind

variations, causing the spectral peak for the total global angular momentum oscillation to have about *50%* more power than that for the relative angular momentum (i.e. wind term) considered separately. An analysis of the cumulus precipitation field shows no intraseasonal periodicity in the total latent heating, confirming that the model oscillation is dynamically- rather than thermodynamically - driven.

Enhanced AAM power is also evident at periods of 16-24 days in spectra of wind variations from both the NH extratropics and the tropics The global AAM, in particular, has a strong maximum in this band, with the full (relative plus planetary) angular momentum showing a sharp peak at 21 days. A westward-traveling wave with about this frequency has been observed in NH data at 500 mb and at other levels, especially at high latitudes, by Branstator (1987') and Kushnir (1987). Ghil and Mo (1991a,b) have also studied an oscillation in this frequency range using NH 700 mb data, tropical OLR data and SH 500 mb data; Hartmann et al. (1992) have detected oscillations in the 20-25 day range in the Western Pacific. In addition, theoretical studies (Tribbia and Ghil 1990) have shown that nonlinear interaction with these higher-frequency variations may play an important role in the generation of 40-50 day oscillations.

Examination of a 12-year record of AAM data derived from the NMC operational analysis showed that a statistically significant oscillation with a period near 40 daya exists in the NH extratropics, distinct from a larger, So-day AAM oscillation found in the tropics (Dickey et al. 1991). These findings increase our confidence in the realism of the GCM oscillation, and indicate that two distinct intraseasonal oscillations may exist in the global angular momentum budget: a 50-day tropical variation, presumably associated with the Madden-Julian oscillation (e.g. Madden 1987; Benedict and Haney 1988; Lau et al, 1989), and a smaller but

distinct 40-day oscillation, which appears to arise from the nonlinear interaction of topography with the large-scale flow field in the extratropics.

Variations in the extratropics make only a small contribution to the global 40-50 day oscillation in atmospheric angular momentum (AAM) and length-of-day (LOD), which is dominated by zonal wind fluctuations between 20S and 20N (e.g. Benedict and Haney 1988; Gutzler and Madden 1993). In a case study of the strongest LOD oscillations on record, however, Dickey et al. (1991) showed that the largest 36-60 day tropical AAM and LOD variations, occurring in early 1988, were preceded by intense intraseasonal AAM oscillations in the NH extratropics during the fall of 1987. These findings, along with further results to be discussed in Part 11 of this study, indicate that extratropical disturbances of the type documented here in the UCLA GCM maybe capable of exciting intraseasonal variability in the tropics. The extent to which the NH oscillations are affected by feedbacks from the tropics, and how these feedbacks would be modified by the inclusion of the Madden-Julian oscillation in the model, will be the subject of future investigations.

Acknowledgments. It is a pleasure to acknowledge discussions with A. Arakawa and C. R. Mechoso on the UCLA GCM. K. Weickmann suggested a closer look at the zonally symmetric pressure oscillations in the tropics. J. Spahr helped with the runs and extracting the requisite output fields. This work was supported at UCLA by NSF grant ATM90-13217 and NASA grant NAG5-317. The work of S.L.M. and J.O.D. is the result of one phase of research carried out at the Jet Propulsion Laboratory, California Institute of Technology, sponsored by the National Aeronautics and Space Administration.

References

Anderson, J. A., and R. D. Rosen, 1983: The latitude-height structure of 40-50 day variations in atmospheric angular momentum. *J. Atmos. Sci.*, 40, 1583-1591.

Arakawa, A., and V. R. Lamb, 1981: A potential enstrophy and energy conserving scheme for the shallow water equations. Mon. *Wea. Rev.*, 109, 674-701.

Arakawa, A., and M. J. Suarez, 1983: Vertical differencing of the primitive equations in sigma coordinates. *Mon. Wea. Rev.*, 111, 34-35,

Barnes, R. T. H., R. Hide, A. A. White, and C. A. Wilson, 1983: Atmospheric angular momentum fluctuations correlated with length of day changes and polar motion, *Proc. R. Sot. London Ser. A., 387, 31-73.*

Benedict, W. L., and R. L. Haney, 1988: Contribution of tropical winds to subseasonal fluctuations in atmospheric angular momentum and length of day. *J. Geophys. Res.*, 93, 15973-15978.

Branstator, G., 1987: A striking example of the atmosphere's leading traveling pattern. *J. Atmos. Sci., 44,* 2310-2323.

Brillinger, D. R., 1975: *Tim Series: Data Analysis and Theory,* HoIt, Reinhart and Winston, New York.

Dickey, J. O., T. M. Eubanks, and J. A. Steppe, 1986: High accuracy Earth rotation and atmospheric angular momentum. In *Earth Rotation: Solved and Unsolved Problems*, A. Cazenave (cd.), D. Reidel, Dordrecht, 137-162.

Dickey, J. O., M. Ghil, and S. L. Marcus, 1991: Extratropical aspects of the 40-50 day oscillation in length-of-day and atmospheric angular momentum. *J. Geophys. Res.*, 96, 22643-22658.

Eubanks, T. M., J. A. Steppe, J. O. Dickey, and P. S. Callahan, 1985: A spectral analysis of the Earth's angular momentum budget. *J. Geophys. Res., 90, 5385-5404.*

Gao, X. H., and J. L. Stanford, 1988: Possible feedback path for low-frequency atmospheric oscillations. *J. Atmos. Sci.*, 45, 1425-1432.

Ghil, M., 1987: Dynamics, statistics and predictability of planetary flow regimes. In *Irreversible Phenomena and Dynamical Systems Analysis in Geosciences, C.* Nicolis and G. Nicolis (eds.), D. Reidel, Dordrecht, 241-283.

Ghil, M., 1988: Nonlinear approaches to low-frequency variability. In *Dynamics ofLow-Frequency Phenomena in the Atmosphere, G.* Branstator, R. Madden and J. Tribbia, (eds.), pp. 603-714, NCAR, Boulder, CO 80307.

Ghil, M., and S, Childress, 1987: *Topics in Geophysical Fluid Dynamics: Atmospheric Dynamics, Dynamo Theory, and Climate Dynamics.* Springer-Verlag, Berlin/New York/Tokyo, 485 pp.

Ghil, M., and K Mo, 1991a: Intraseasonal oscillations in the global atmosphere, Part I, Northern hemisphere and tropics. *J. Atmos. Sci..*, 48, 752-779,

Ghil, M., and K Mo, 1991b: Intraseasonal oscillations in the global atmosphere, Part 11, Southern hemisphere. *J. Atmos. Sci..*, 48, 780-790.

Goswami, B. N., and J. Shukla, 1984: Quasi-periodic oscillations in a symmetric general circulation model. *J. Atmos. Sci.*, 41, 20-37.

Gutzler, D. S., and R. A. Madden, 1993: Seasonal variations of the 40-50 day oscillation in atmospheric angular momentum. *J. Atmos. Sci, SO,* 850-860.

Hartmann, D. L., M. L. Michelsen, and S. A. Klein, 1992: Seasonal variations of tropical intraseasonal oscillations: a 20-25 day oscillation in the western Pacific, *J. Atmos. Sci.*, 49, 1277-1289.

Hayashi, Y., and A. Sumi, 1986: The 30-40 day oscillations simulated in an "aqua planet" model. *J. Meteorol. Sot. Jpn., 64, 451-467,*

Hayashi, Y., and D. G. Golder, 1993: Tropical 40-50- and 25-30-day oscillations appearing in realistic and idealized GFDL climate models and the ECMWF dataset. *J. Atmos. Sci. SO,* 464-494.

Hide, R., 1977: Towards a theory of irregular variations in the length of day and core-mantle coupling. *Philos. Trans. R. Sot. London Ser. A, 2$4, 547-554.*

Hide, R., and J. O. Dickey, 1991: Earth's variable rotation, Science, 2S3, 629.

Hsu, H.-H., B. J. Hoskins, and F.-F. Jin, 1990: The 1985 / 86 intraseasonal oscillation and the role of the extratropics. *J. Atmos. Sci.*, 47, 823-839.

James, I. N., and P. M. James, 1992: Spatial structure of ultra-low-frequency variability of the flow in a simple atmospheric circulation model. *Quart. J. Roy, Met. Soc.*, 118, 1211-1233.

Jenkins, G. M., and D. G. Watts 1968: *Spectral Analysis and Its Applications*, Holden-Day, San Francisco, *525* pp.

Jin, F.-F., and M. Ghil, 1990: Intraseasonal oscillations in the extratropics: Hopf bifurcation and topographic instabilities. *J. Atmos. Sci.*, 47, 823-839.

Keppenne, C. L., 1989: Bifurcations, strange attractors, and low-frequency atmospheric dynamics, Ph. D. Thesis, 158 pp., University Catholique & Louvain.

Knutson, T. R., and K. M. Weickmann, 1987: 30-60 day atmospheric oscillations: composite life cycles of convection and circulation anomalies. Mon. *Wea. Rev.*, 115, 1407-1436.

Kousky, V. E., 1988: Zonally-averaged fluctuations in tropical sea level pressure. *Trop. Ocean-Atmos. Newsl.*, *6-8*, August, 1988.

Kushnir, Y., 1987: Retrograding wintertime low-frequency disturbances over the North Pacific Ocean. *J. Atmos. Sci.*, *44*, 2727-2742.

Lambeck, K, 1980: The *Earth's variable Rotation*, Cambridge Univ. Press, London and New York.

Langley, R. B., R. W. King, I. I. Shapiro, R. D. Rosen, and D. A. Salstein, 1981: Atmospheric angular momentum and the length of the day: a common fluctuation with a period near 50 days. *Nature,* 294, 730-733.

Lau, N. C., and K M. Lau, 1986: Structure and propagation of intraseasonal oscillations appearing in a GFDL GCM, *J. Atmos. Sci.*, 43, 2023-2047,

Lau, K M., and L Peng, 1987: Origin of low-frequency (intraseasonal) oscillations in the tropical atmosphere. Part 1. Basic theory. *J. Atmos. Sci., 44, 950-972.*

Lau, K. M., and T. J. Phillips, 1986: Coherent fluctuation of extratropical geopotential height and tropical convection in intraseasonal time scales. *J. Atmos. Sci.*, 43, 1164-1181.

Lau, K. M., 1. S. Kang and P. J. Sheu, 1989: Principal modes of intraseasonal variation in atmospheric angular momentum and tropical convection. *J. Geophys. Res, 94,* 6319-6332.

Legras, B., and M. Ghil, 1985: Persistent anomalies, blocking, and variations in atmospheric predictability. *J. Atmos. Sci.*, 42, 433-471.

Lorenc, A. C., 1984: The evolution of planetary-scale 200mb divergent flow during the FGGE year. *Quart. J. Roy, Meteor. Sot.,* 110, 427-441,

Madden, R. A., 1987: Relationships between changes in the length of day and the 40- to 50-day oscillation in the tropics *J. Geophys. Res.*, 92, 8391-8399.

Madden, R. A, 1988: Large intraseasonal variations in wind stress over the tropical Pacific. J. Geophys. Res., 93, 5333-5340.

Madden, R. A., and P. R. Julian, 1971: Detection of a 40-50 day oscillation in the zonal wind in the tropical Pacific. *J. Atmos. Sci., 28,* 702-708.

Madden, R. A., and P. R. Julian, 1972: Description of global-scale circulation cells in the tropics with a 40-50 day period. *J. Atmos. Sci.*, 29, 1109-1123.

Marcus, S. L., 1990: Intraseasonal oscillations in the Earth-atmosphere system, Ph.D. thesis, 184 pp., Univ. of Calif. at Los Angeles.

Mechoso, C. R., A. KitOh, S. Moorthi, and A. Arakawa, 1987: Numerical simulations of the atmospheric response to a sea-surface temperature anomaly over the equatorial eastern Pacific ocean. *Mon. Wea. Rev.*, 11S, 2936-2956.

Pitcher, E. J., and J. E. Geisler, 1987: The 40- to 50-day oscillation in a perpetual January simulation with a general circulation model. *J. Geophys. Res.*, 9211971-11978.

Rosen, R. D., and D.A. Salstein, 1983: Variations in atmospheric angular momentum on global and regional scales and the length of day. *J. Geophys. Res., 88,* 5451-5470.

Simmons, A. J., J. M. Wallace, and G. W. Branstator, 1983: Barotropic wave propagation and instability and atmospheric teleconnection patterns, *J. Atmos. Sci.*, 40, 1363-1392, 1983.

Strong, C. M, F.-F, Jin, and M. Ghil, 1993: Intraseasonal variability in a barotropic model with seasonal forcing. *J. Atmos. Sci*, in press.

Suarez, M. J., A. Arakawa, and D. A. Randall, 1983: The parameterization of the planetary boundary layer in the UCLA general circulation model: Formulation and results. Mon. *Wea. Rev.*, 111, *2224-2243.*

Tokioka, T., K. Yamazaki, A. Kitoh, and T. Ose, 1988: The equatorial 30-60 day oscillation and the Arakawa-Schubert penetrative cumulus parametrization, *J. Met. Sot, Japan, 66, 883-901.*

Tribbia, J. J., and M. Ghil, 1990: Forced zonal flow over topography and the 30-60 day oscillation in atmospheric angular momentum. *NCAR* 0502/89-5, 26 pp., National Center for Atmospheric Research, Boulder, Colorado.

Vautard, R., and M. Ghil, 1989: Singular spectrum analysis in nonlinear dynamics, with applications to paleoclimatic time series. Physics, 35D, 395-424.

Weickmann, K. M., S. J. S. Khalsa, and J. Eischeid, 1992: The atmospheric angular momentum cycle during the tropical Madden-Julian Oscillation, Men, *Wea. Rev.*, 120, 2252-2263.

Table 1: No-Mountain Experiments

Run #	Radiation Code	Boundary Conditions	Duration
1	standard	standard	300 days
2	standard	ENSO	380 days
3	revised	standard	350 days

Figure Captions

Fig. 1. (a) Zonally-averaged northern hemisphere surface temperature for days 1-37o (solid line), days 371-740 (dashed line), and days 741-1120 (dotted line) of the standard-topography run. (b) As in (a), for the zonally-averaged mass-weighted zonal velocity.

Fig. 2. Deviation of the AAM of the model atmosphere from its mean value during the standard run, in LOD units. Results are shown for the global domain (upper panel), and separately (lower three panels) for the NH extratropics (20N-90N), the tropics (20S-20N), and the SH extratropics (90S-20S).

Fig. 3. AutoCorrelation estimate for AAM from the standard model computed for the global domain, and separately for the NH extratropics, the tropics, and the SH extratropics.

Fig. 4. Log-log power spectra of AAM from the model run, computed for the global domain, and separately for the NH extratropics and the tropics. Each is fitted to an AR 1 model (middle smooth curves) with 95% confidence levels shown (upper and lower smooth curves). The bandwidth on these spectra and subsequent ones having logarithmic abscissa pertains only to the frequency at which it is plotted.

Fig. S. Log-linear power spectra of AAM from the standard model, computed separately for the NH extratropics and the tropics; the power spectrum for the tropical region has been adjusted to compensate for the effect of its greater mean axial distance on the AAM variance.

Fig. 6. Cross-correlation estimate for AAM from the standard model, between the tropics and NH extratropics, the SH extratropics and the tropics, and the SH extratropics and NH extra tropics. Approximate 95% confidence intervals are given by the horizontal dotted lines.

Fig. 7. (a) Time series of AAM from the standard model filtered in the 36-60 day band, for the global domain (dotted) and the NH extratropics (solid). (b) The envelope of the NH extratropical oscillation from (a), computed by complex demodulation.

Fig. 8. AutoCorrelation estimate for the model AAM from the NH extratropics, computed separately for each quarter of the standard-topography run.

Fig. 9. (a) Sea-surface temperature (SST) anomaly used for the second no-mountain experiment. The SST data were taken from January 1983, representing the warm phase of the El Niño/Southern Oscillation. The contour interval is 1°K, with solid (dashed) curves indicating warmer (colder) temperatures starting at 0.5 (-0.5) oK. (b) Surface temperature difference between the first and third no-mountain experiments. The solid curves show cooling produced by the modified radiation scheme, using a contour interval of 2°K.

Fig. 10. (a) Average zonal velocity in the NH extratropics for the four GCM experiments (see Table 1), weighted by mass and the cosine of the latitude. The three no-mountain experiments were initialized with the same state as the standard-topography experiment, leading to transient oscillations for about the first 40 days. Each curve is given an arbitrary vertical offset to allow for clearer presentation, (b) AutoCorrelation estimates for NH extratropical AAM from the four GCM experiments. The first 40 days of the no-mountain runs were dropped to eliminate transients, and only days 1-300 were considered from the standard experiment, The standard-topography run shows a clear secondary maximum in

the 40-50 day range, while the three no-mountain experiments show no evidence of periodicity in the intraseasonal band.

Fig. 11. (a) Power spectrum of average 500 mb height in the tropics; (b) power spectrum of the average surface pressure. Note similar shape of the spectra (amplitudes have been normalized), indicating the barotropic nature of the tropical oscillation in the standard-topography run.

Fig. 12. (a) Fluctuations in the total mass content of the NH extratropics and the tropics for the standard-topography run, filtered in the 36-60 day band. (b) Power spectra of the total mass content of the NH extratropics and tropics.

Fig. 13. (a) Log-1 inear power spectra of the global wind term and global pressure term from the standard-topography run, plotted in LOD units. (b) As in (a), where the wind term is restricted to the NH extratropics, and plotted on a different scale.

Fig. 14. (a) Cross-correlation between 36-60 day fluctuations in the wind term and total mass content of the NH extratropics during the standard-topography run. (b) Composites of zonally-averaged atmospheric mass and relative angular momentum keyed to the 36-60 day filtered time series of NH extratropical AAM. The dashed curve represents the difference between high and low AAM states, corresponding to days when the filtered AAM anomaly exceeded 1.5 times its standard deviation. The solid curve gives the difference in mass distribution between low and high NH AAM states (the sign reversal simplifies the presentation), The zonal rms deviation of the model surface topography is shown in arbitrary units on the bottom axis for comparison.

Fig. 15. Log-linear power spectra of the total AAM (solid line) and wind term only (dotted line) for the standard-topography run. Note the large enhancements in spectral power for the total AAM at periods of 43.5 and 21 days, due to coherent contributions from the pressure term.

Fig. 16. (a) **Autocorrelation** estimates for the average surface pressure (solid) and cumulus heating (dashed) from the model tropics. (b) **Log-log** power spectrum for the average tropical cumulus precipitation, for periods from ***3 to 300 days; (c)*** as in (b), using log-linear **coordinates** for periods between 10 and 100 days.

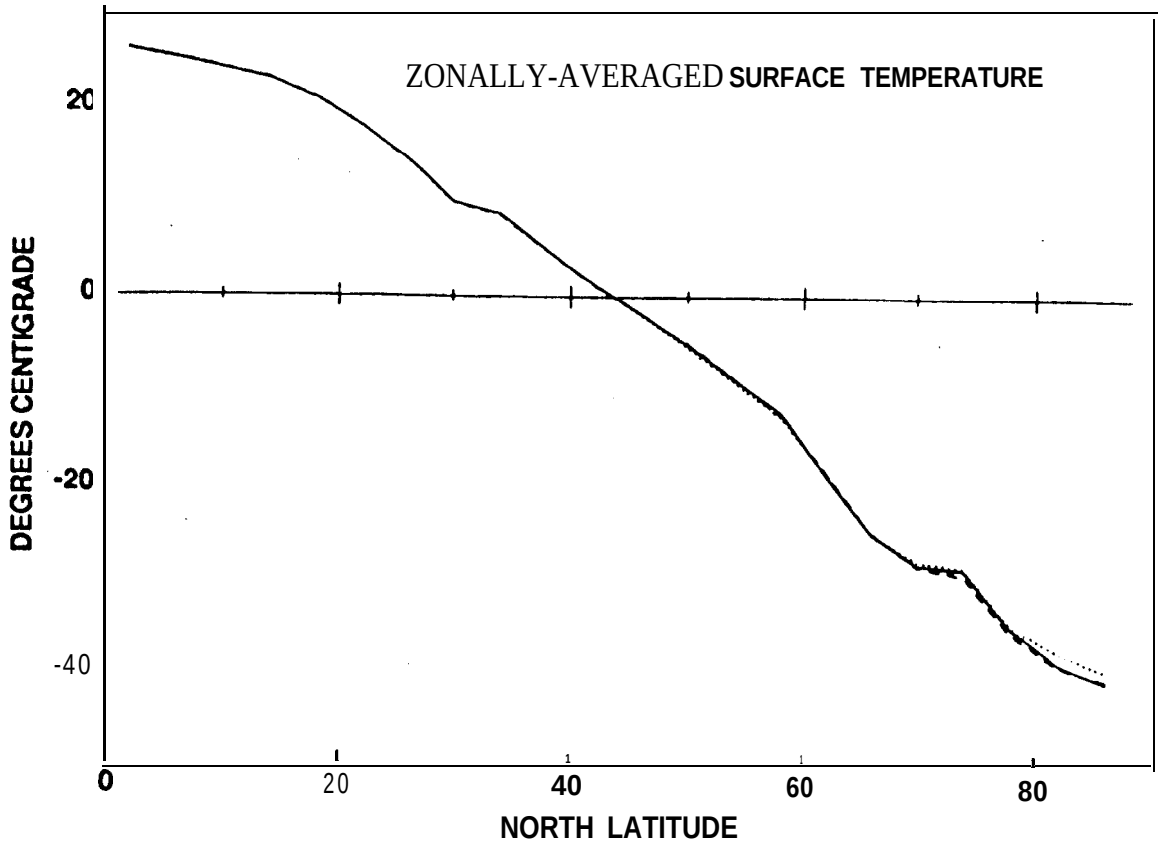
ZONALLY-AVERAGED SURFACE TEMPERATURE
DEGREES CENTIGRADE
20
0
-20
-40
0
20
40
60
80
NORTH LATITUDE

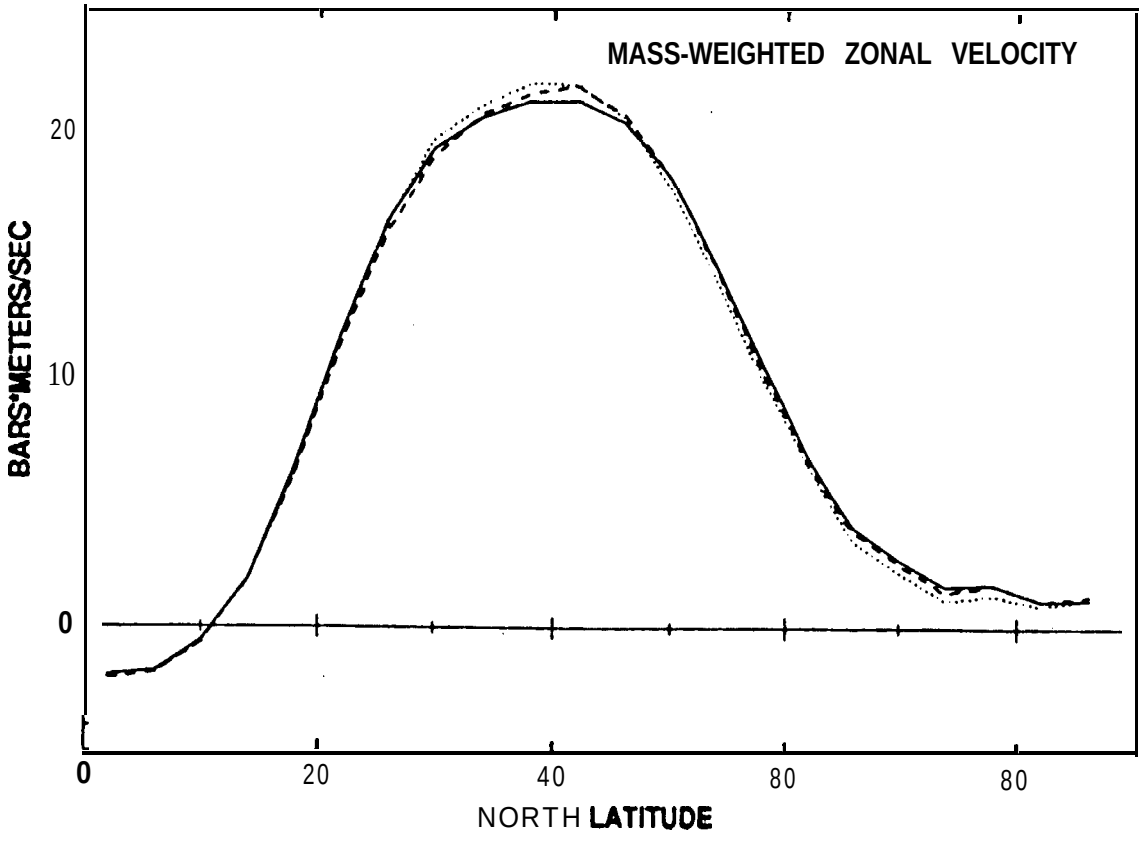
MASS-WEIGHTED ZONAL VELOCITY
BARS*METERS/SEC
20
10
0
0
20
40
80
80
NORTH LATITUDE

Fig. 1

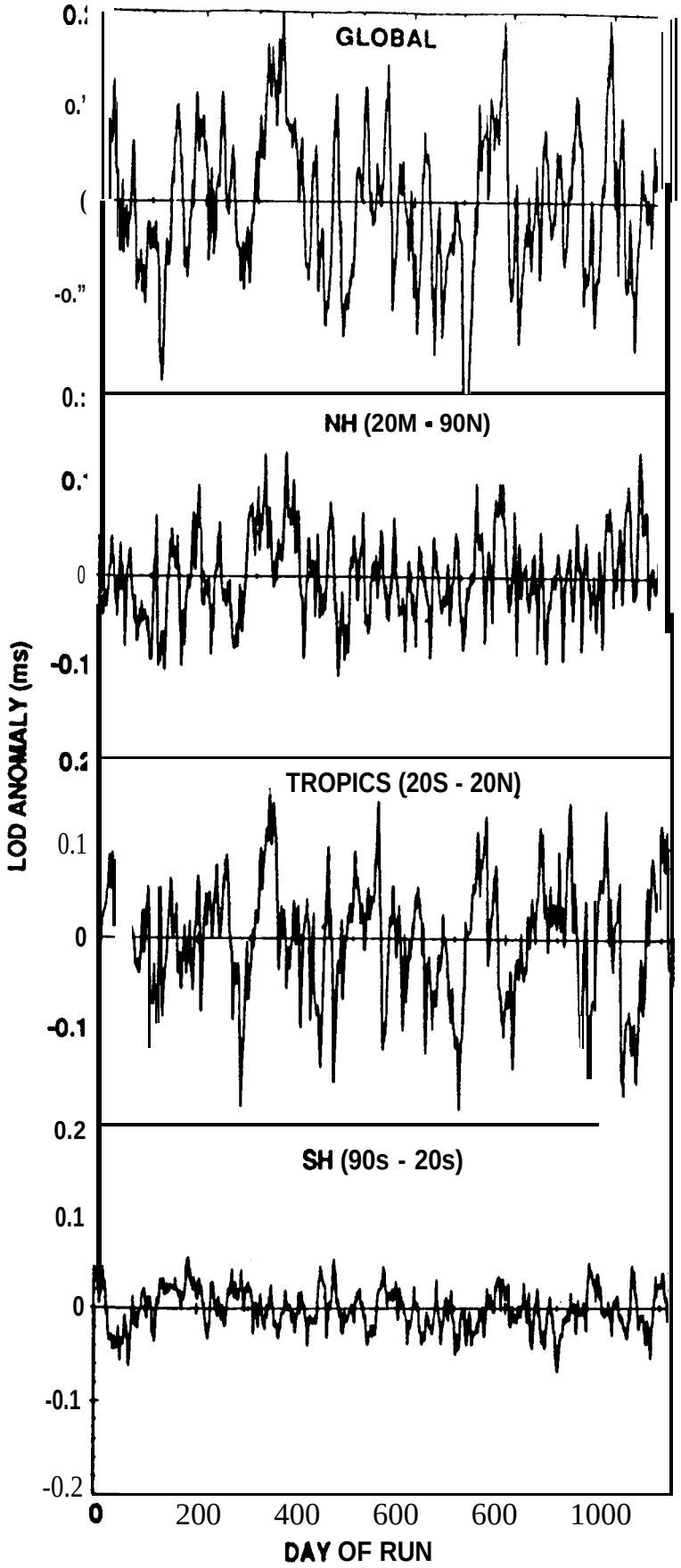
GLOBAL
NH (20M - 90N)
TROPICS (20S - 20N)
SH (90s - 20s)
LOD ANOMALY (ms)
0.1
0
-0.1
0.2
-0.2
0
200
400
600
600
1000
DAY OF RUN

Fig. 2

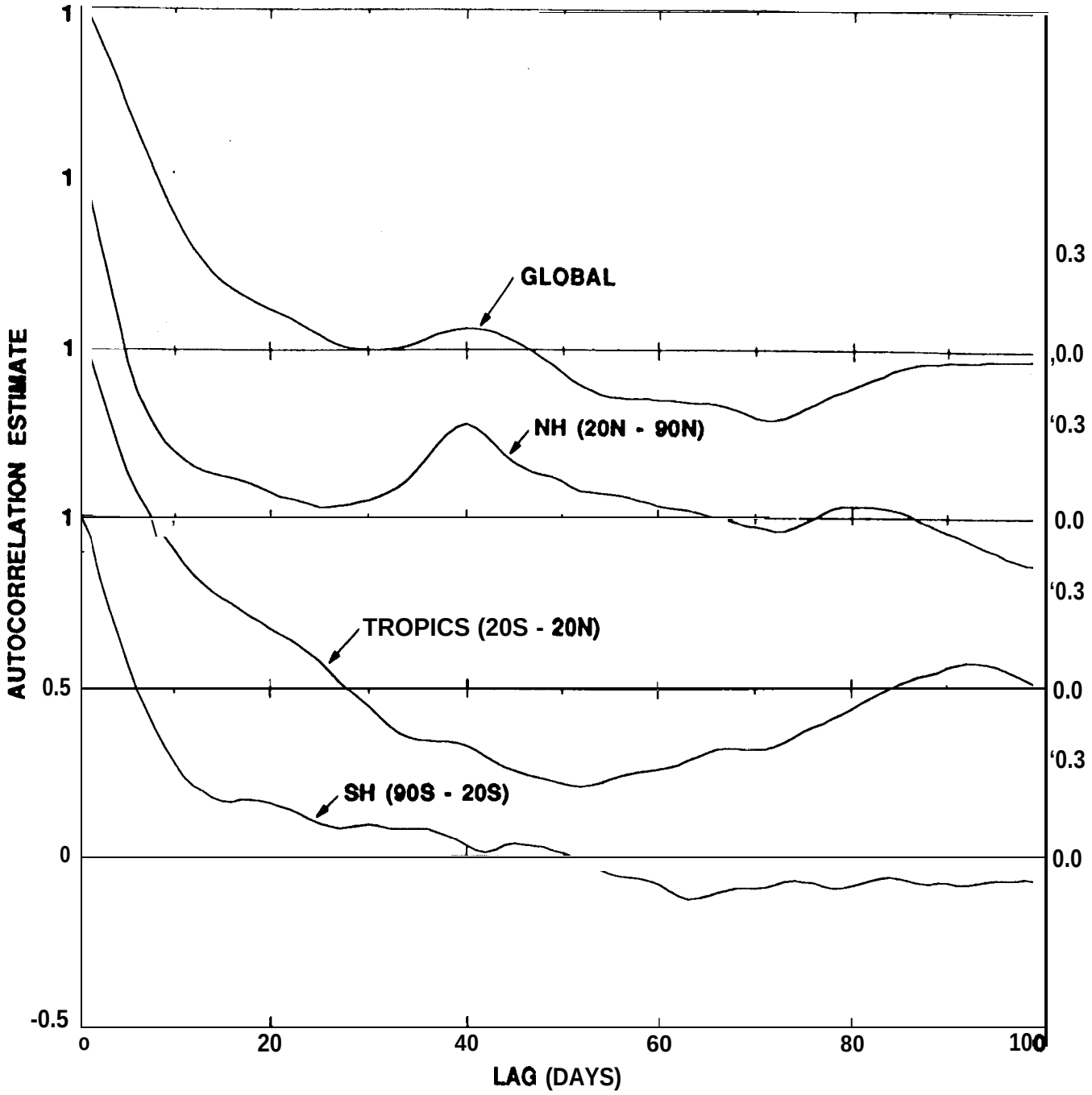
AUTOCORRELATION ESTIMATE
1
1
1
1
0.5
0
-0.5
GLOBAL
NH (20N - 90N)
TROPICS (20S - 20N)
SH (90S - 20S)
0.3
,0.0
'0.3
0.0
'0.3
0.0
'0.3
0.0
0
20
40
60
80
100
LAG (DAYS)

Fig. 3

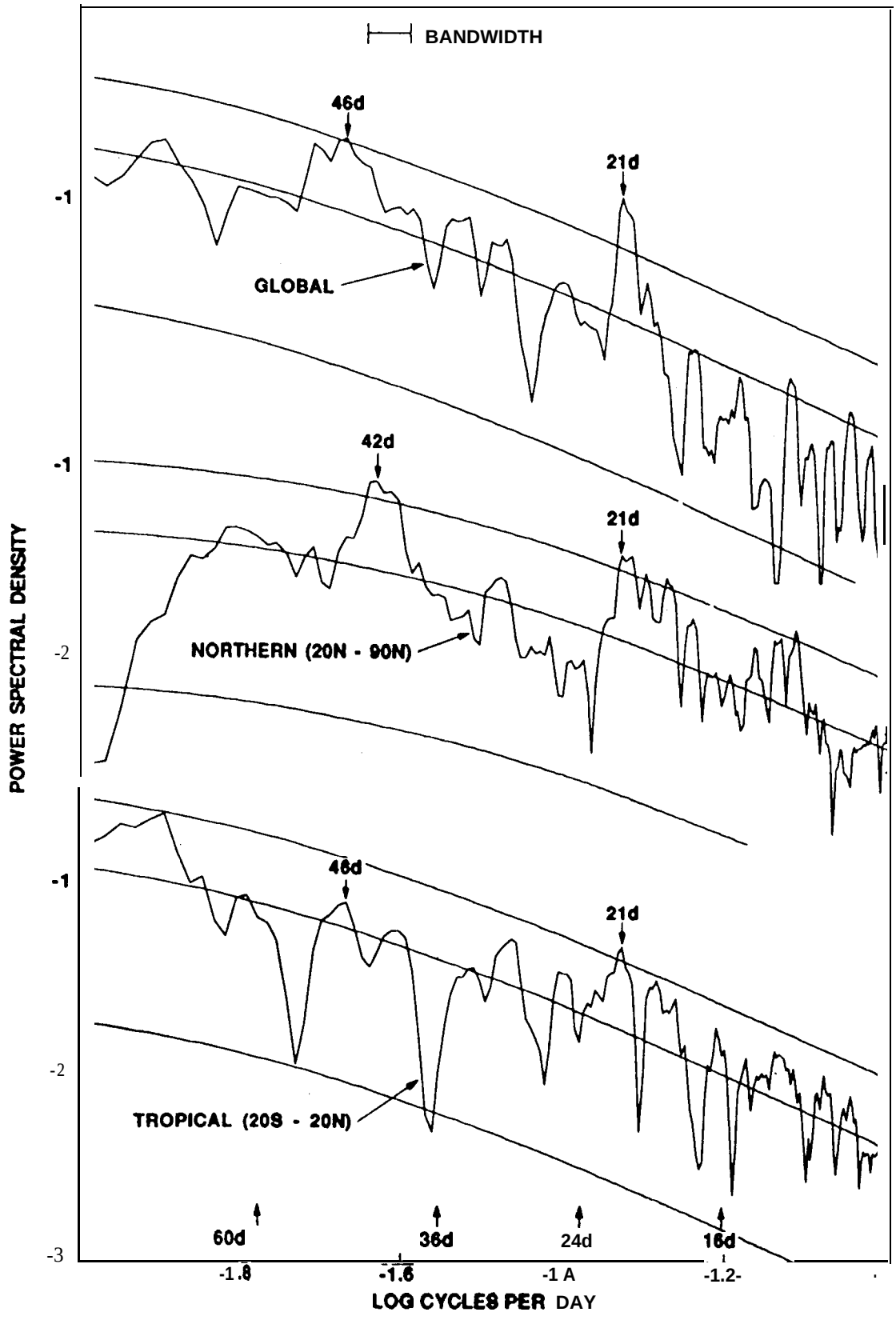
BANDWIDTH
46d
21d
GLOBAL
42d
21d
NORTHERN (20N - 90N)
46d
21d
TROPICAL (20S - 20N)
60d
36d
24d
16d
-1
-1
-2
-1
-2
-3
POWER SPECTRAL DENSITY
-1.8
-1.6
-1 A
-1.2-
LOG CYCLES PER DAY

Fig. 4

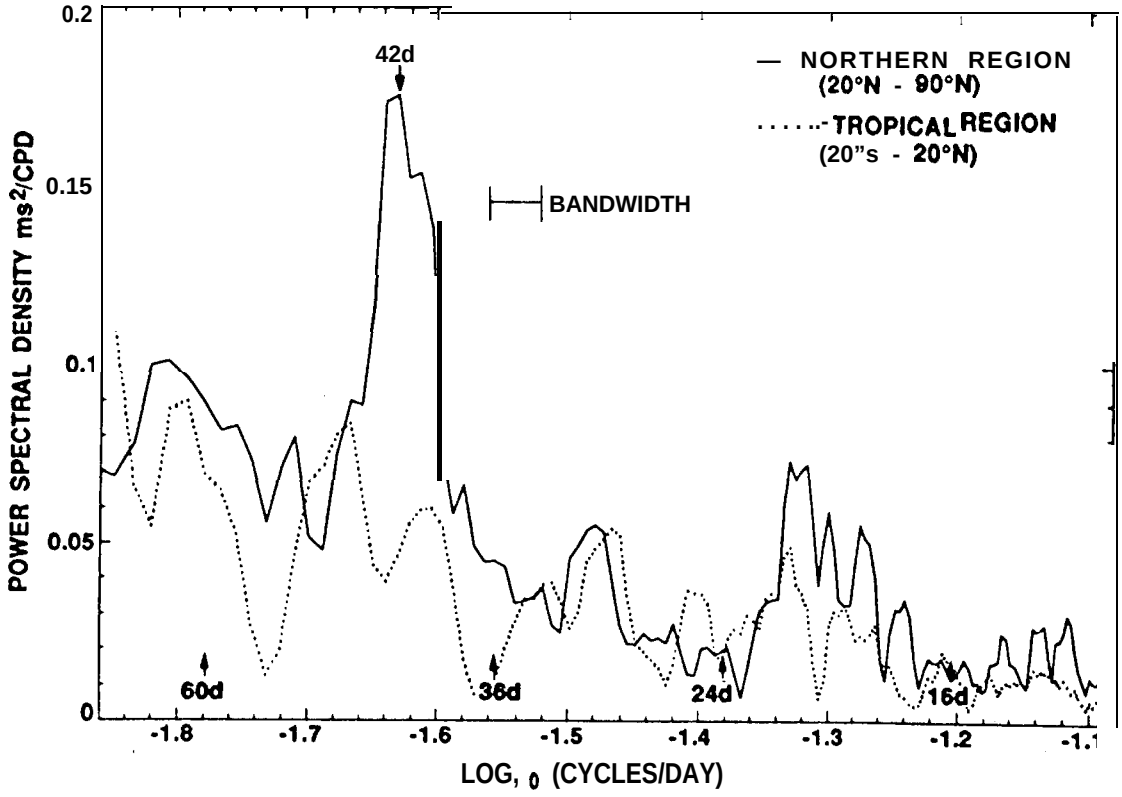
0.2
0.15
0.1
0.05
0
POWER SPECTRAL DENSITY ms²/CPD
42d
— NORTHERN REGION
(20°N - 90°N)
TROPICAL REGION
(20"s - 20°N)
BANDWIDTH
60d
36d
24d
16d
-1.8
-1.7
-1.6
-1.5
-1.4
-1.3
-1.2
LOG, 0 (CYCLES/DAY)

Fig. 5

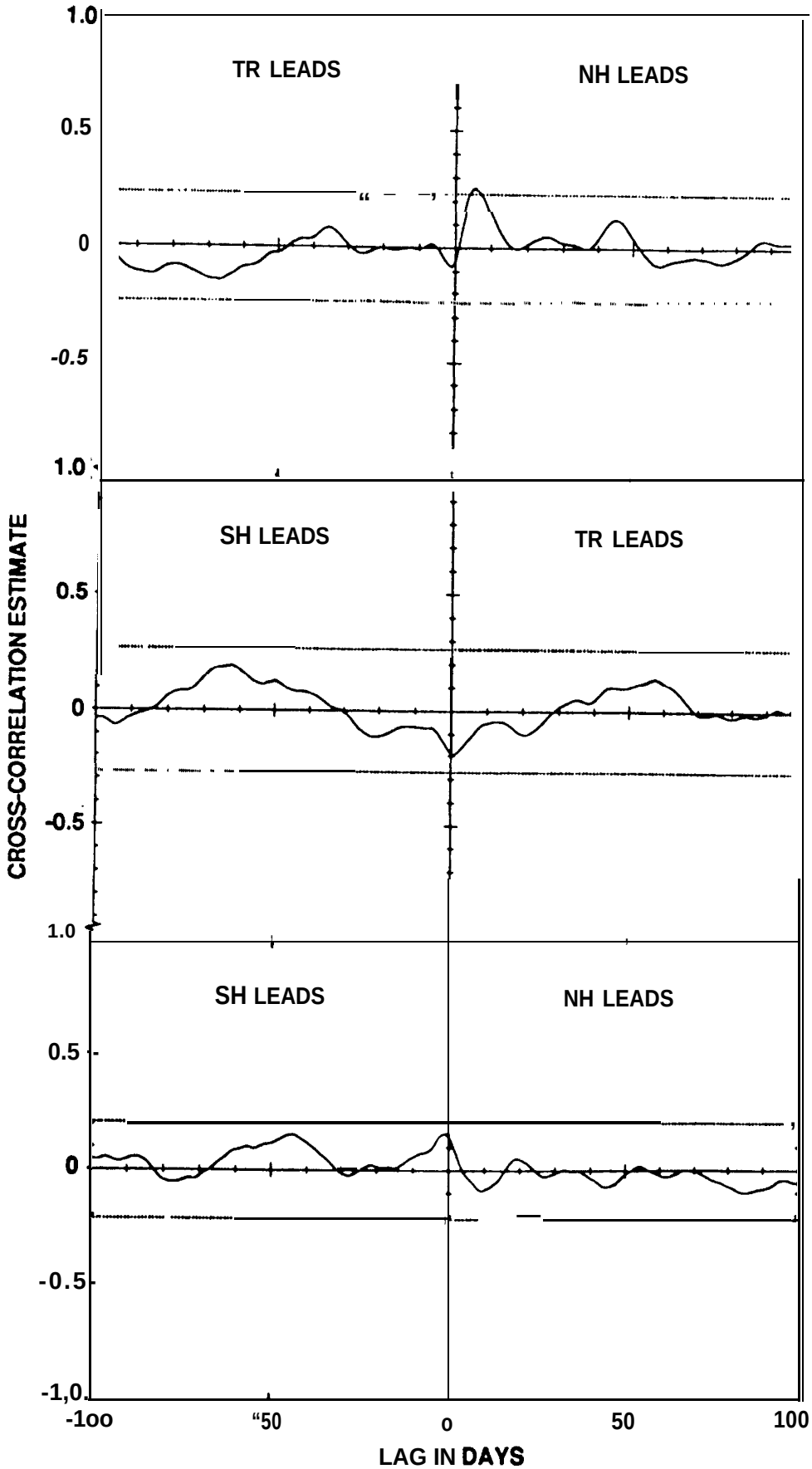
1.0
TR LEADS
NH LEADS
0.5
0
-0.5
1.0
SH LEADS
TR LEADS
0.5
0
-0.5
1.0
SH LEADS
NH LEADS
0.5
0
-0.5
-1,0
-1oo
"50
0
50
100
CROSS-CORRELATION ESTIMATE
LAG IN DAYS

Fig. 6

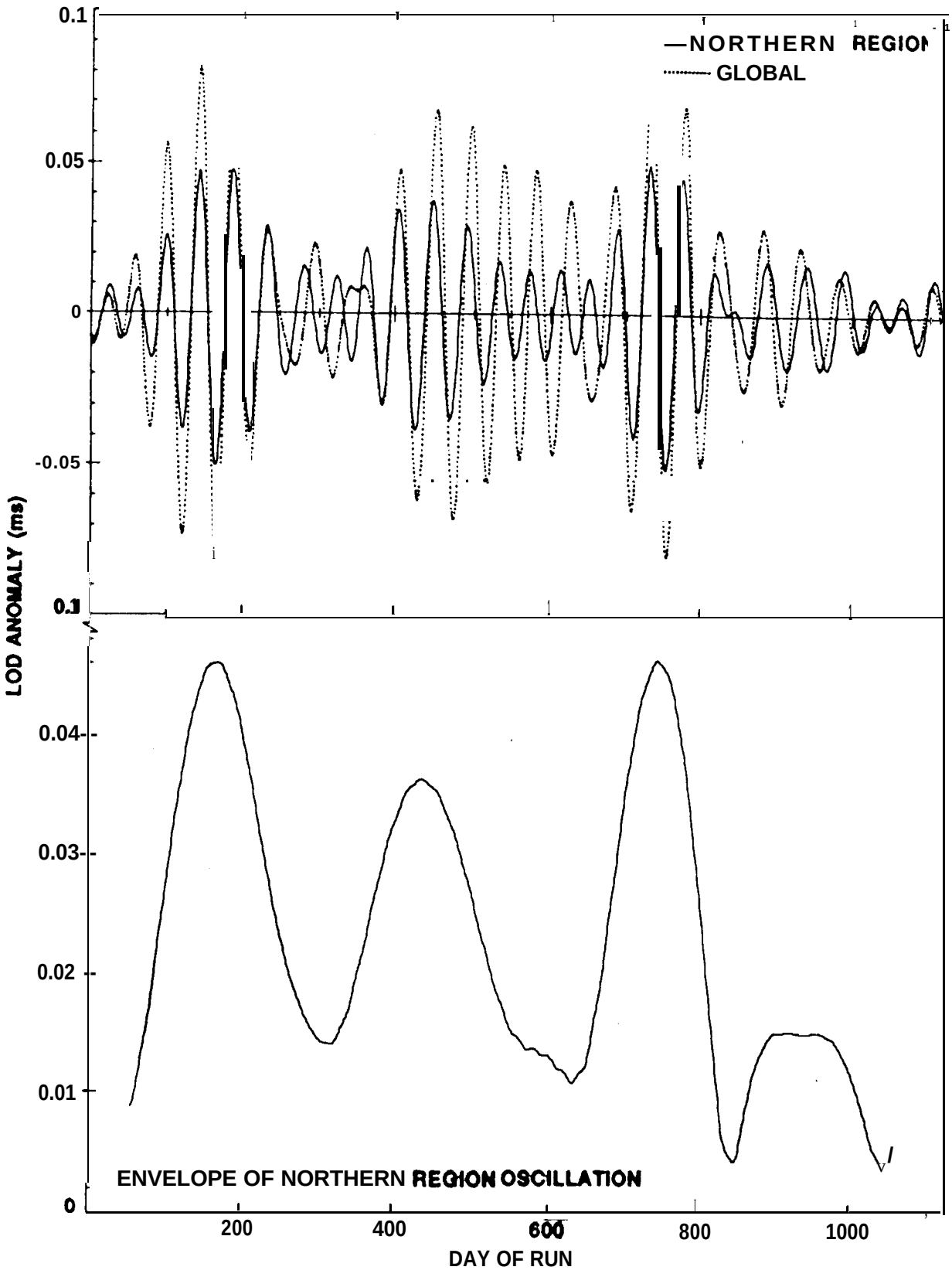
0.1
0.05
0
-0.05
-0.1
—NORTHERN REGION
GLOBAL
LOD ANOMALY (ms)
0.04
0.03
0.02
0.01
0
ENVELOPE OF NORTHERN REGION OSCILLATION
200
400
600
800
1000
DAY OF RUN

Fig. 7

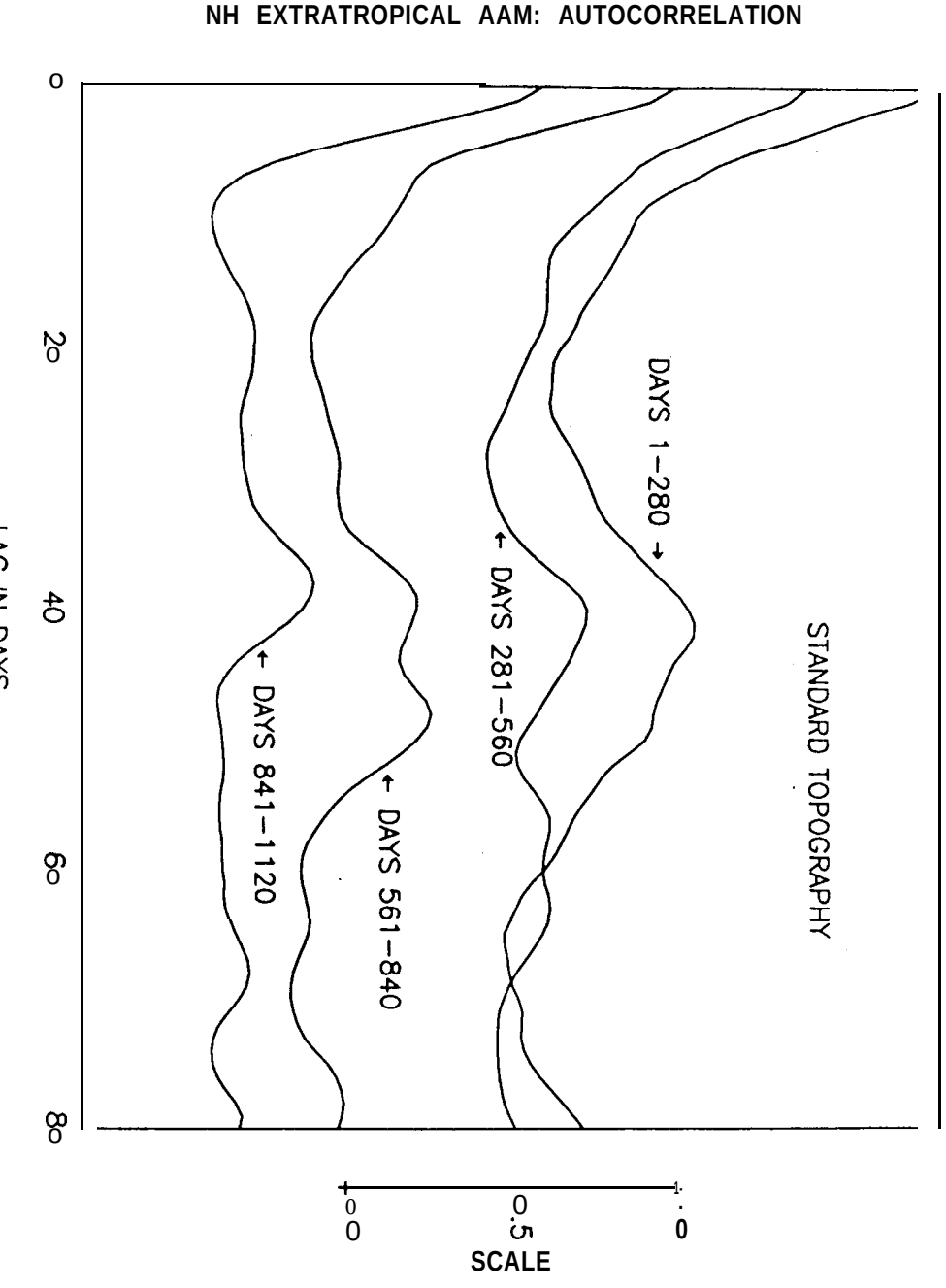
NH EXTRATROPICAL AAM: AUTOCORRELATION
0
20
40
60
80
LAG IN DAYS
DAYS 1–280 →
← DAYS 281–560
← DAYS 561–840
← DAYS 841–1120
STANDARD TOPOGRAPHY
0
0.5
1.0
SCALE

Fig. 8

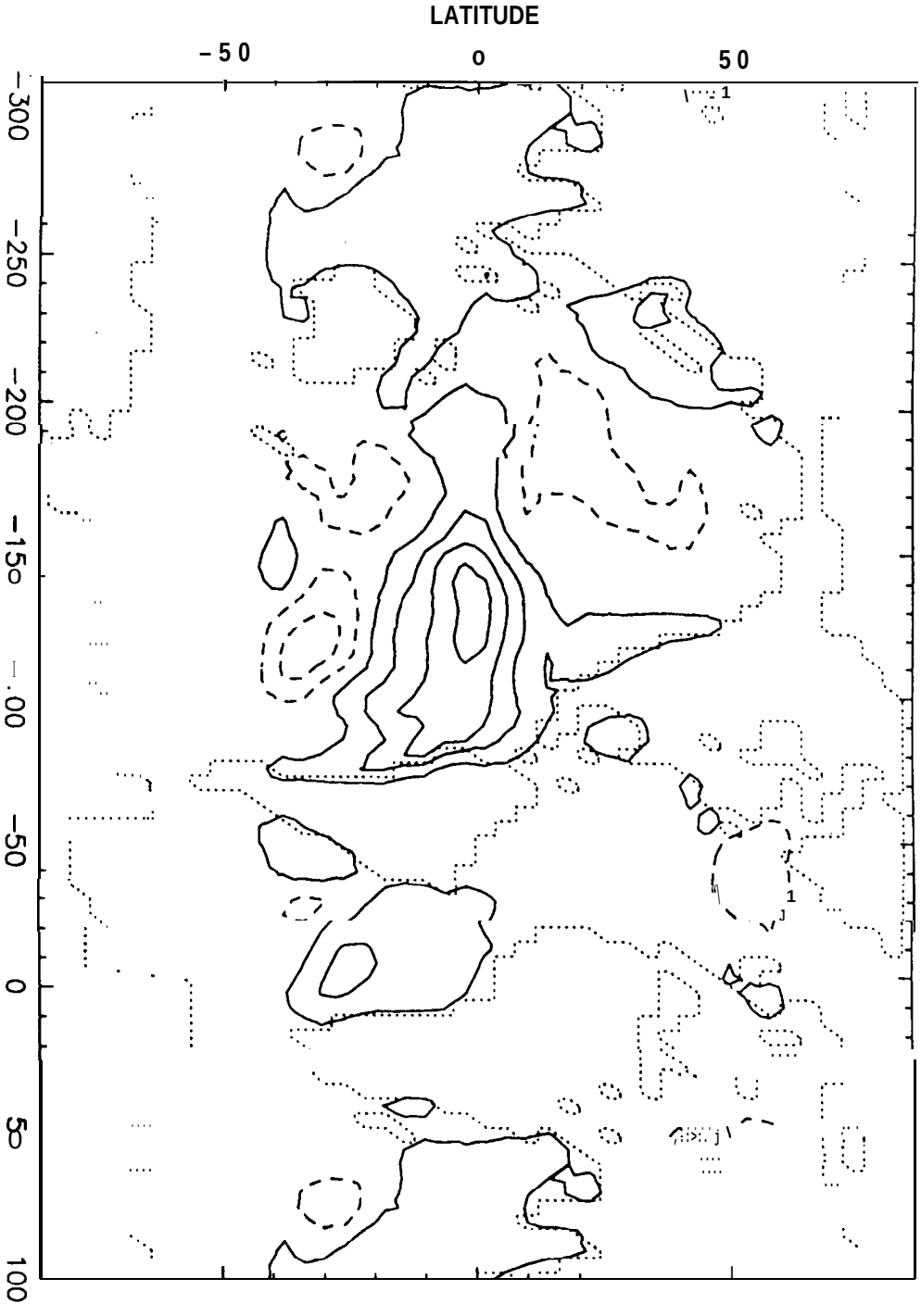

Fig. 9a

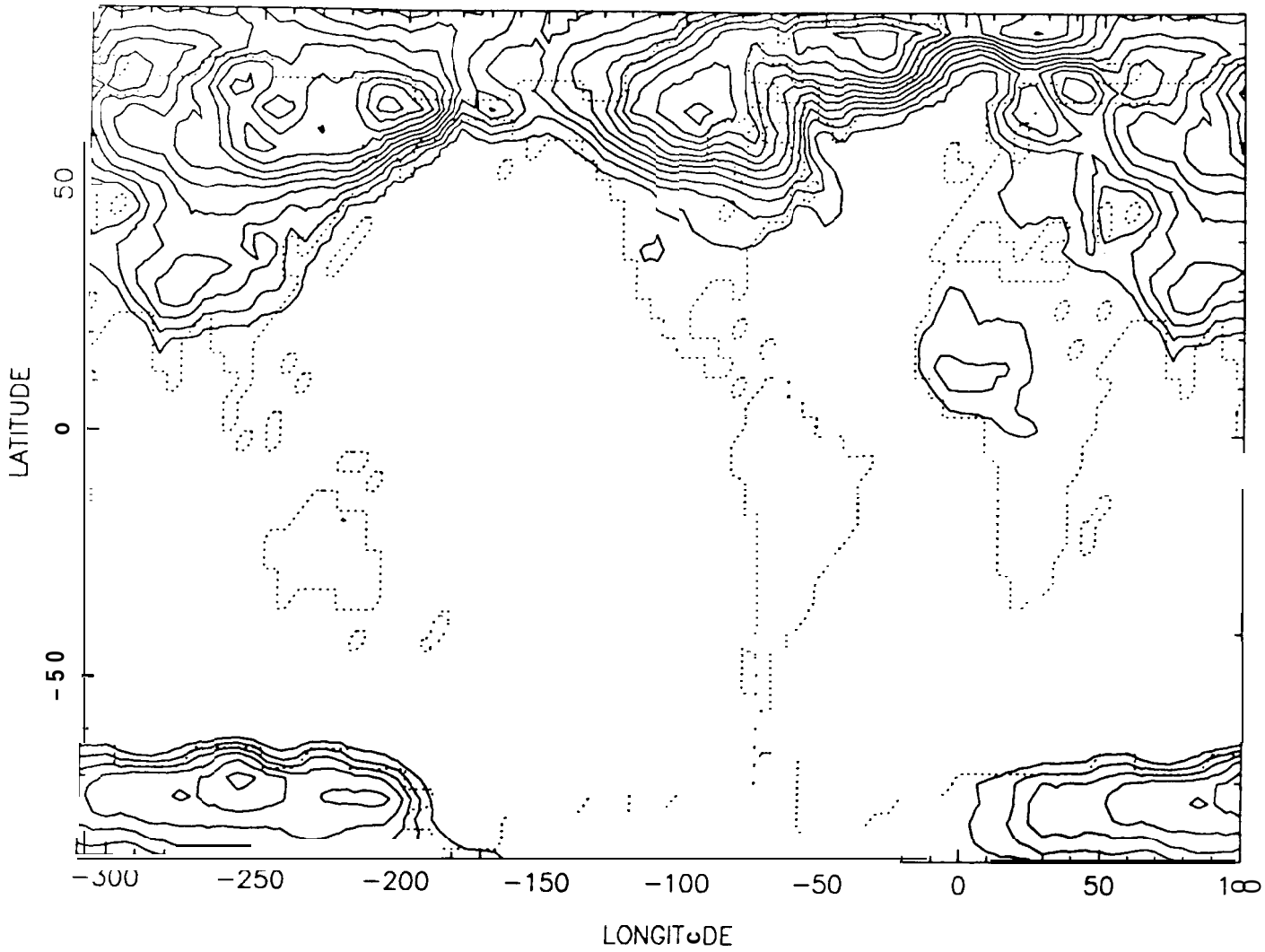

Fig. 9b

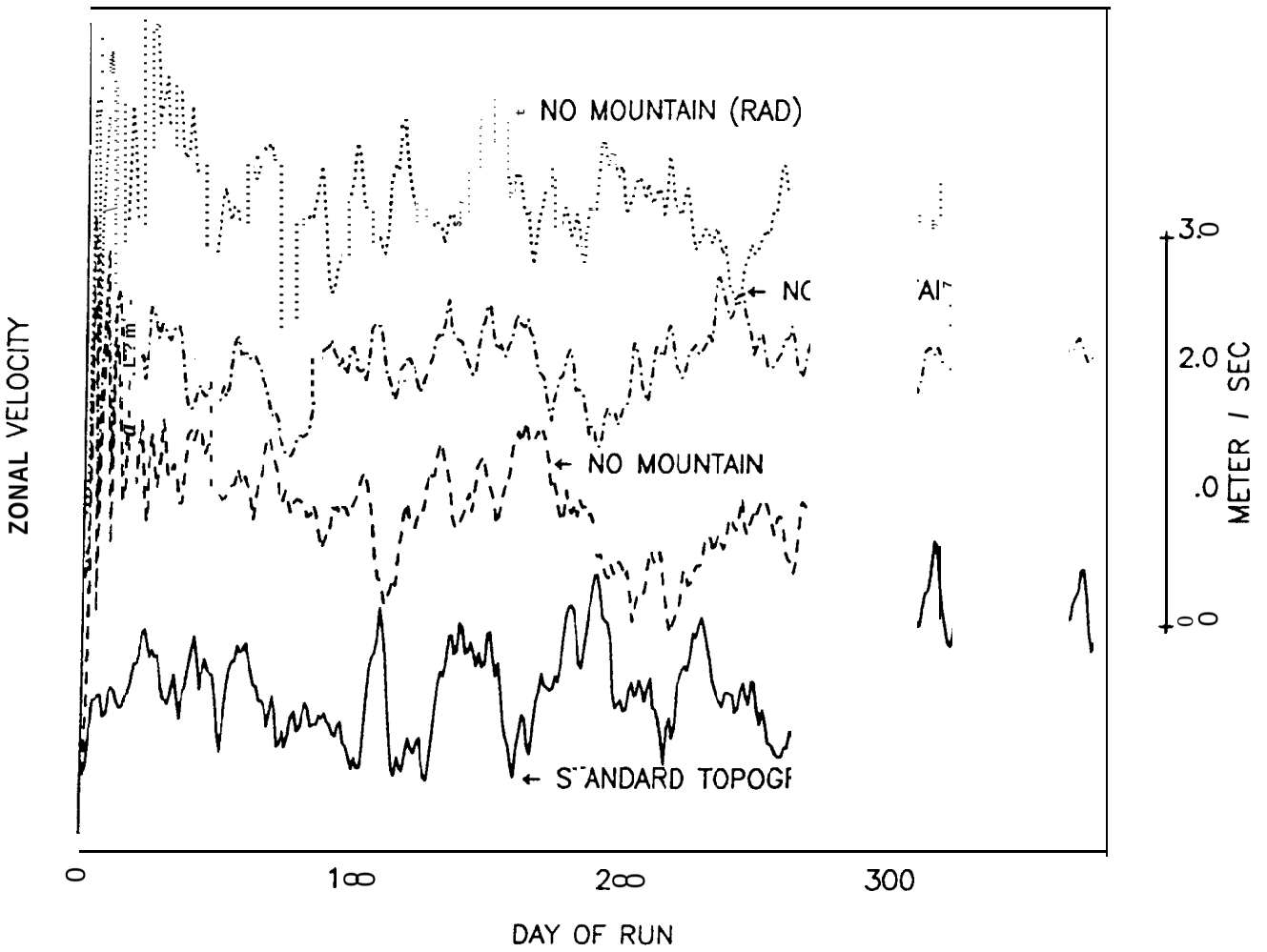
NO MOUNTAIN (RAD)
← NC
AI
← NO MOUNTAIN
← STANDARD TOPOGR
ZONAL VELOCITY
METER / SEC
3.0
2.0
.0
0
0
100
200
300
DAY OF RUN

Fig. 10a

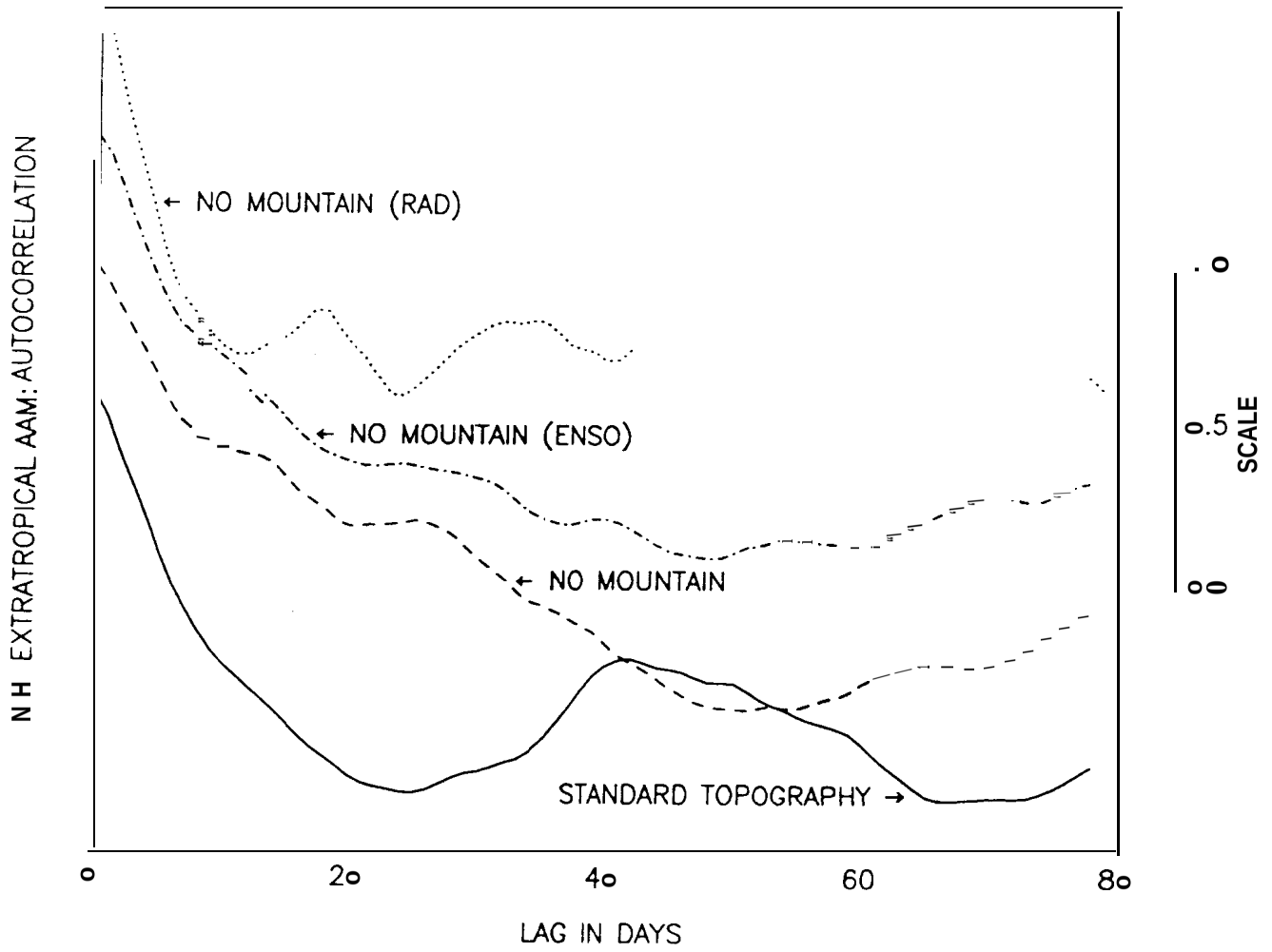
NH EXTRATROPICAL AAM: AUTOCORRELATION
← NO MOUNTAIN (RAD)
← NO MOUNTAIN (ENSO)
← NO MOUNTAIN
STANDARD TOPOGRAPHY →
0
20
40
60
80
LAG IN DAYS
1.0
0.5
0.0
SCALE

Fig. 10

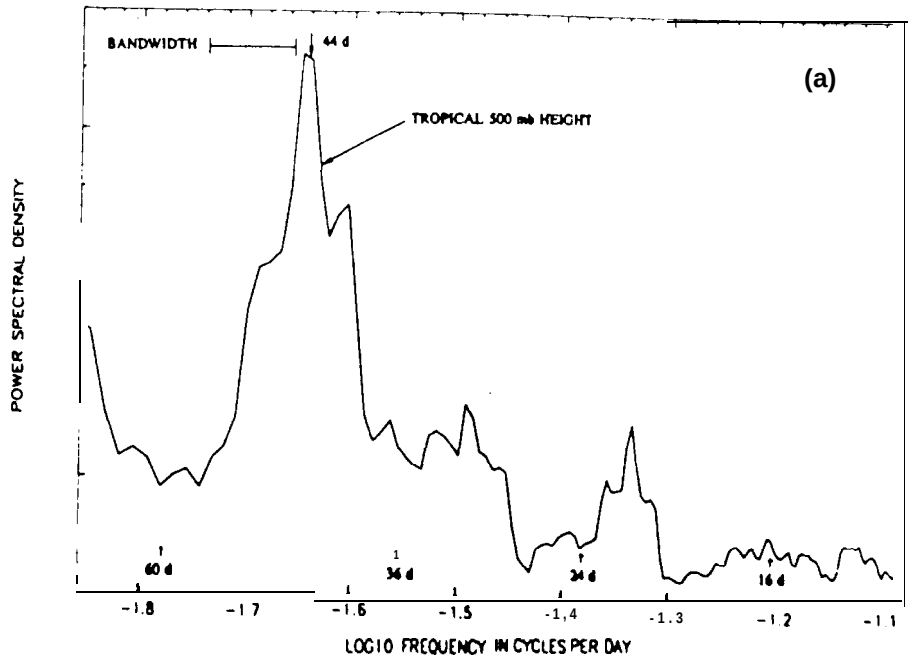
BANDWIDTH
44 d
(a)
TROPICAL 500 mb HEIGHT
POWER SPECTRAL DENSITY
60 d
36 d
24 d
16 d
-1.8
-1.7
-1.6
-1.5
-1.4
-1.3
-1.2
-1.1
LOG10 FREQUENCY IN CYCLES PER DAY

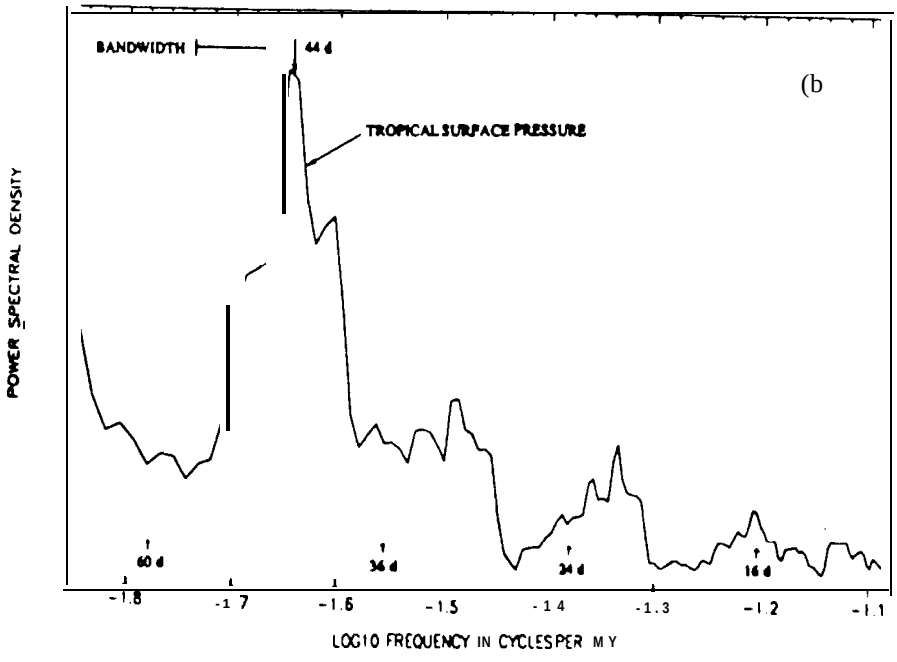
BANDWIDTH
44 d
(b
TROPICAL SURFACE PRESSURE
POWER SPECTRAL DENSITY
60 d
36 d
24 d
16 d
-1.8
-1.7
-1.6
-1.5
-1.4
-1.3
-1.2
-1.1
LOG10 FREQUENCY IN CYCLES PER MY

Fig. 11

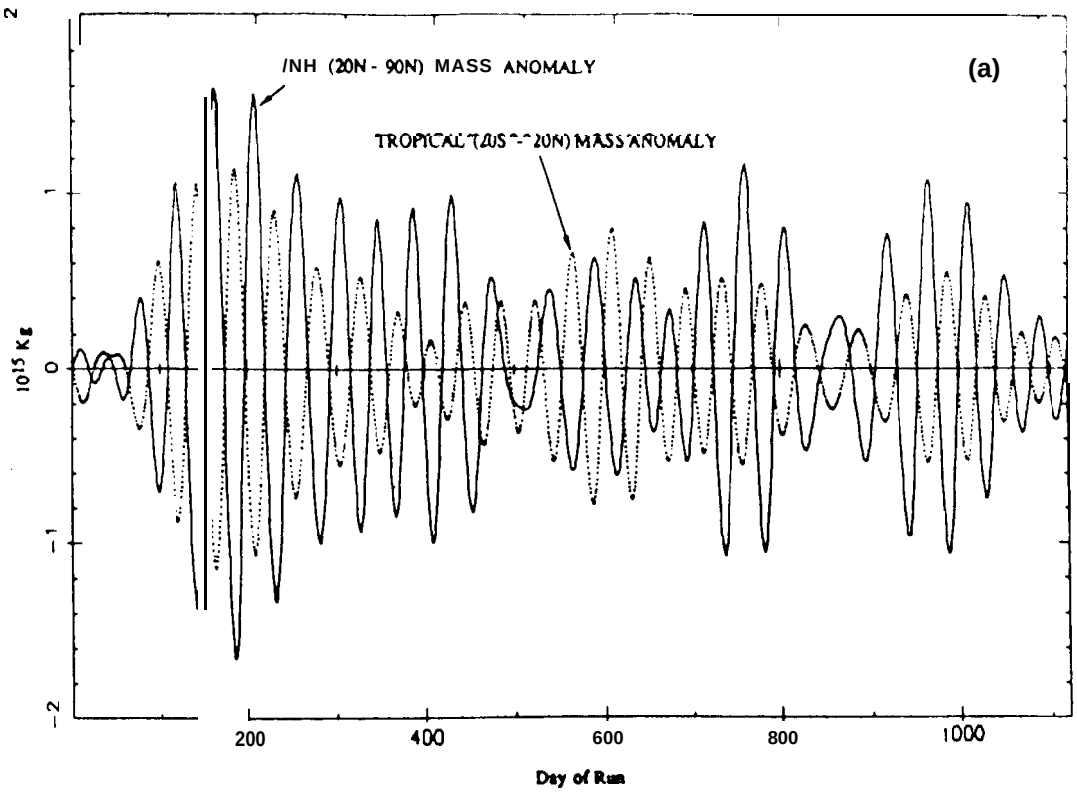
NH (20N - 90N) MASS ANOMALY
(a)
TROPICAL (20S - 20N) MASS ANOMALY
10^{15} Kg
2
1
0
-1
-2
200
400
600
800
1000
Day of Run

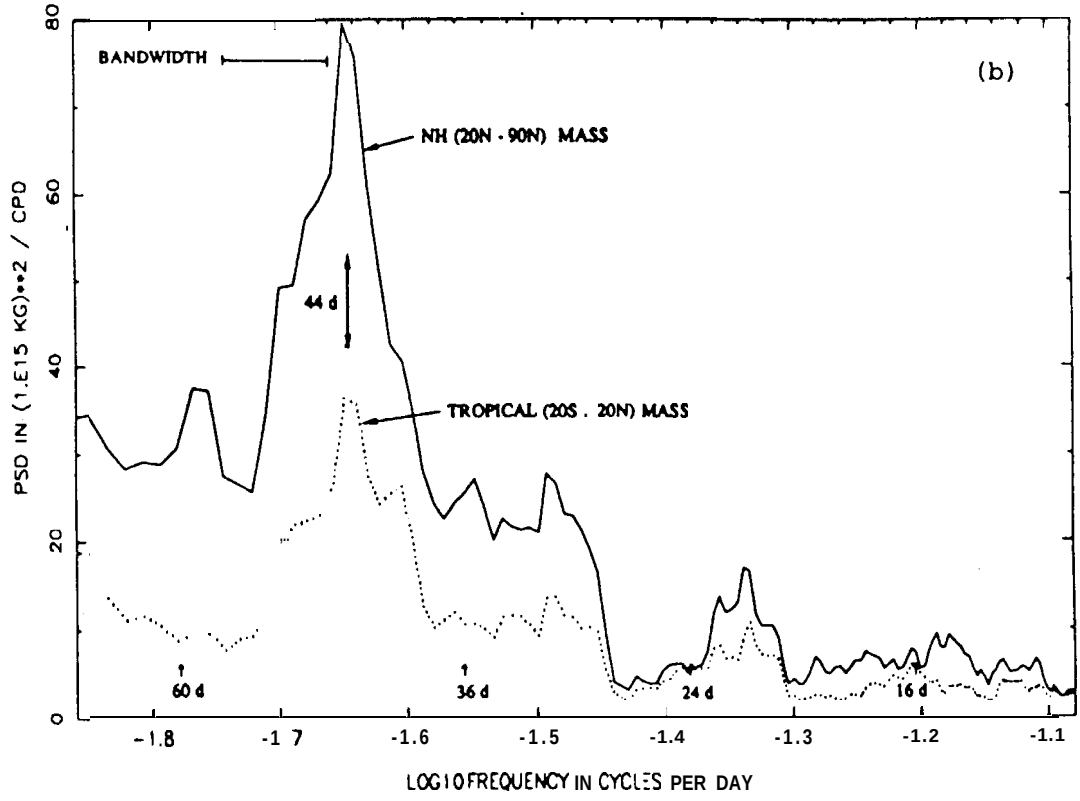
BANDWIDTH
(b)
NH (20N - 90N) MASS
44 d
TROPICAL (20S . 20N) MASS
PSD IN (1.E15 KG)**2 / CPD
80
60
40
20
0
60 d
36 d
24 d
16 d
-1.8
-1 7
-1.6
-1.5
-1.4
-1.3
-1.2
-1.1
LOG10 FREQUENCY IN CYCLES PER DAY

Fig. 12

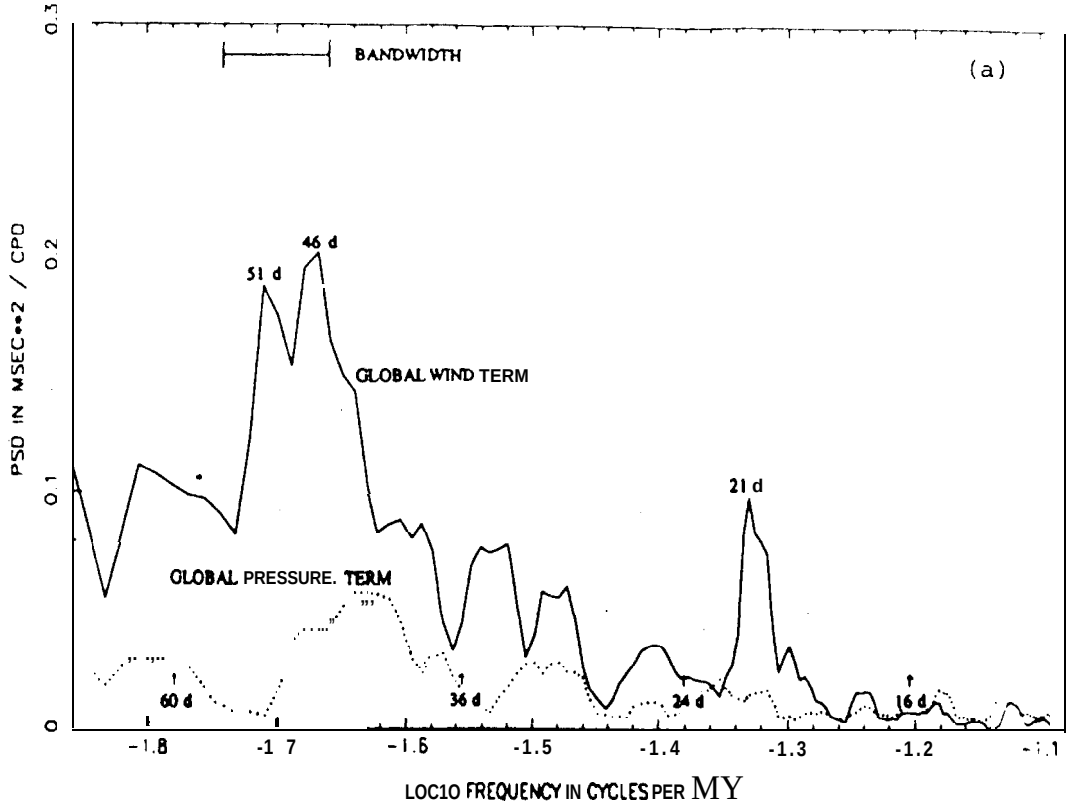
BANDWIDTH
(a)
PSD IN MSEC**2 / CPD
0.3
0.2
0.1
0
46 d
51 d
GLOBAL WIND TERM
21 d
GLOBAL PRESSURE. TERM
60 d
36 d
24 d
16 d
-1.8
-1 7
-1.6
-1.5
-1.4
-1.3
-1.2
-1.1
LOC10 FREQUENCY IN CYCLES PER MY

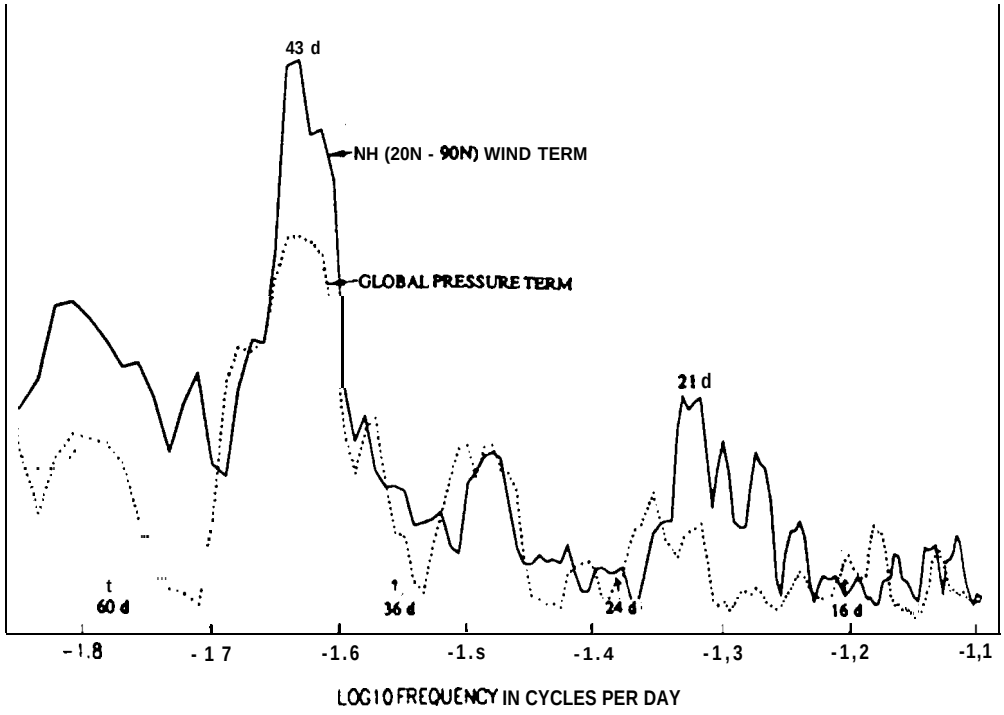
43 d
NH (20N - 90N) WIND TERM
GLOBAL PRESSURE TERM
21 d
60 d
36 d
24 d
16 d
-1.8
- 1 7
-1.6
-1.s
-1.4
-1,3
-1,2
-1,1
LOG10 FREQUENCY IN CYCLES PER DAY

Fig. 13

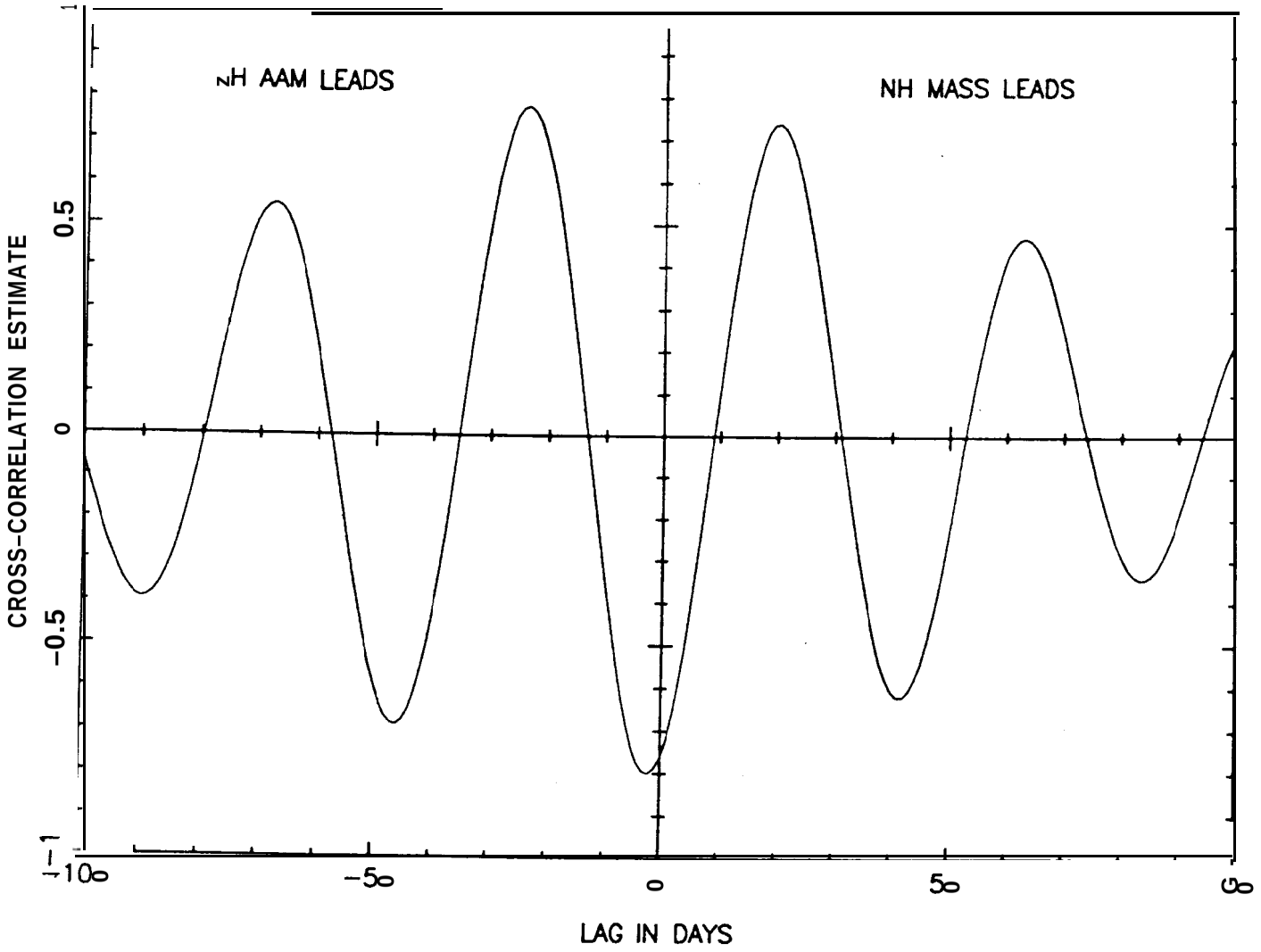
NH AAM LEADS
NH MASS LEADS
CROSS-CORRELATION ESTIMATE
1
0.5
0
-0.5
-1
-10
-5
0
5
10
LAG IN DAYS

Fig. 14a

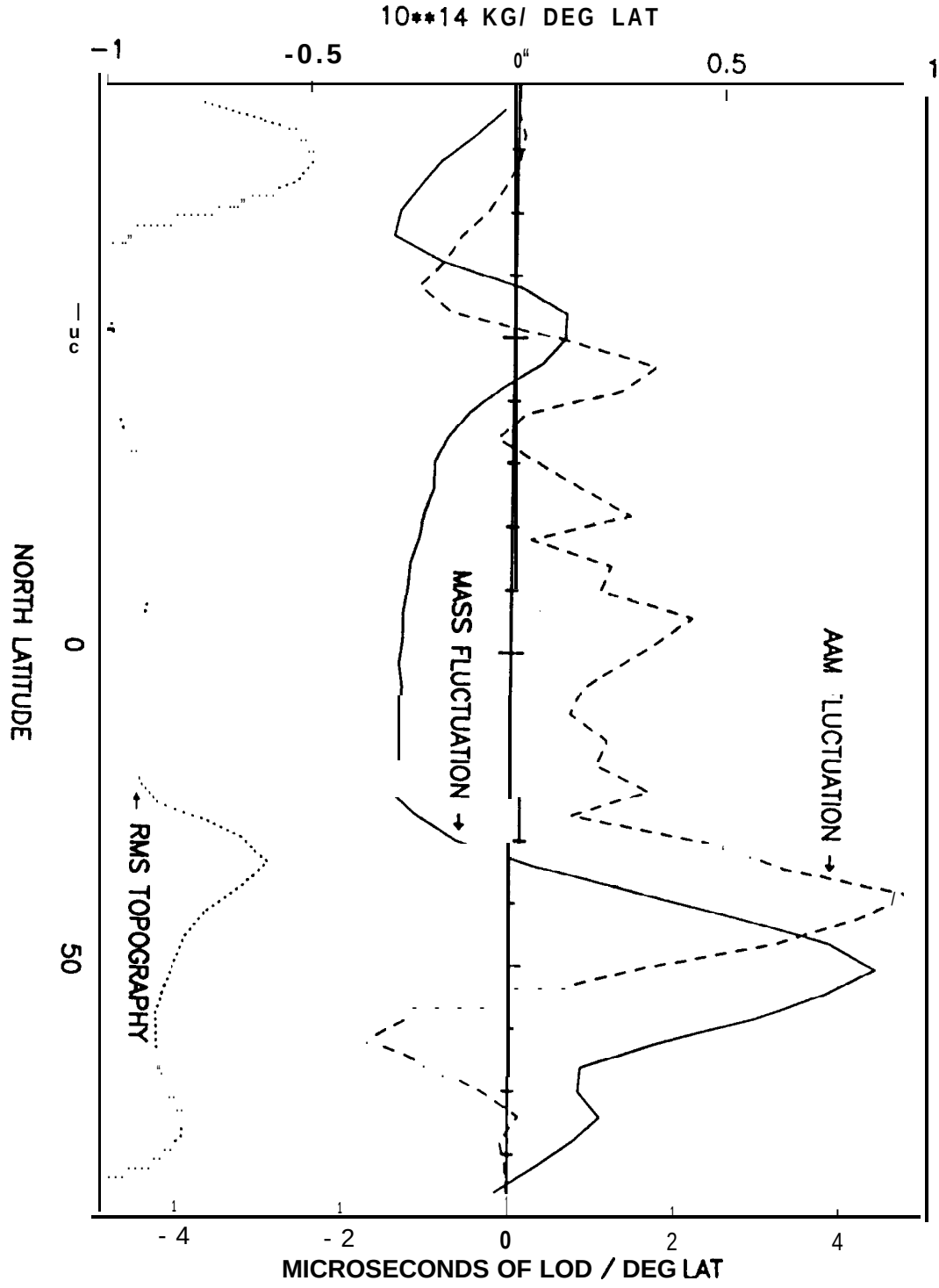
10**14 KG/ DEG LAT
-1
-0.5
0
0.5
1
-90
0
50
NORTH LATITUDE
← RMS TOPOGRAPHY
MASS FLUCTUATION →
AAM FLUCTUATION →
- 4
- 2
0
2
4
MICROSECONDS OF LOD / DEG LAT

Fig. 14b

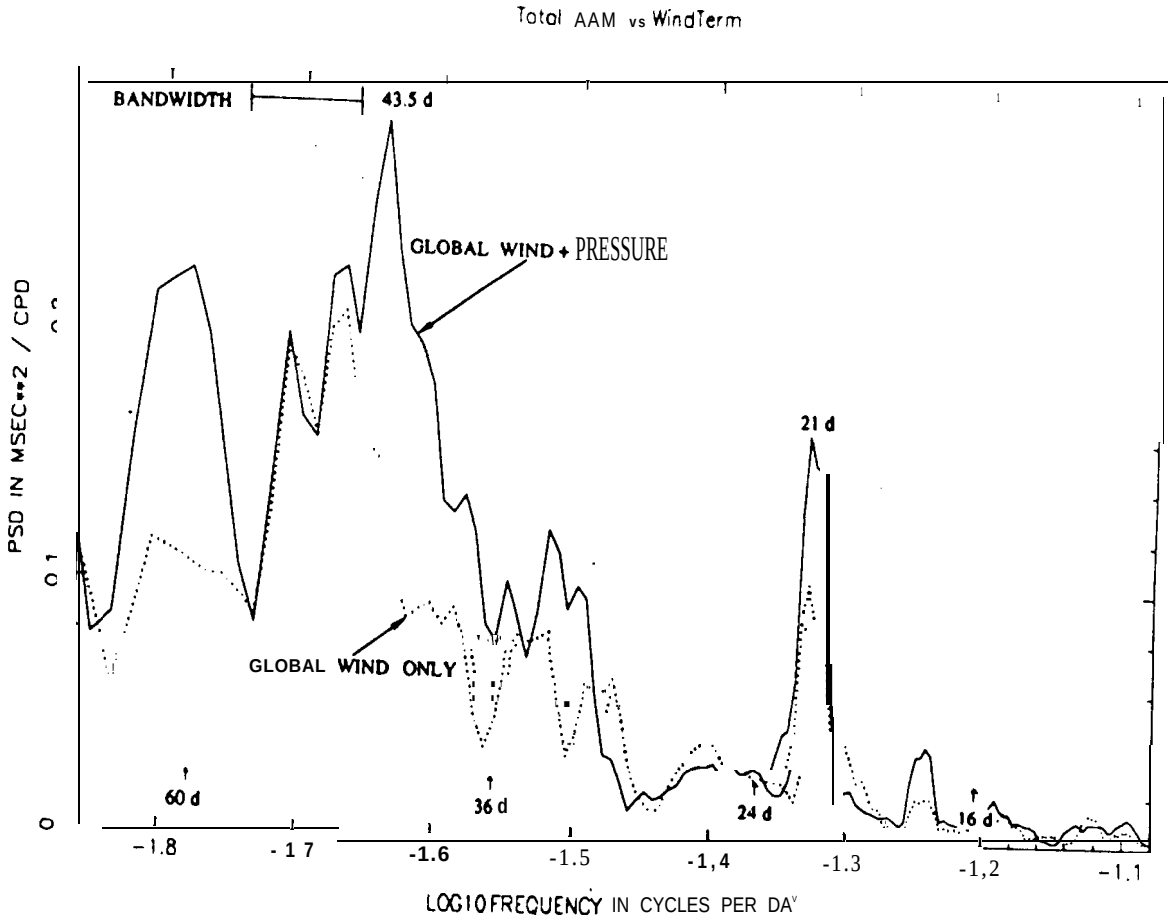
Total AAM vs WindTerm
BANDWIDTH
43.5 d
GLOBAL WIND + PRESSURE
GLOBAL WIND ONLY
21 d
60 d
36 d
24 d
16 d
PSD IN MSEC**2 / CPD
0.1
0
-1.8
-1.7
-1.6
-1.5
-1.4
-1.3
-1.2
-1.1
LOG10 FREQUENCY IN CYCLES PER DAY

Fig. 15

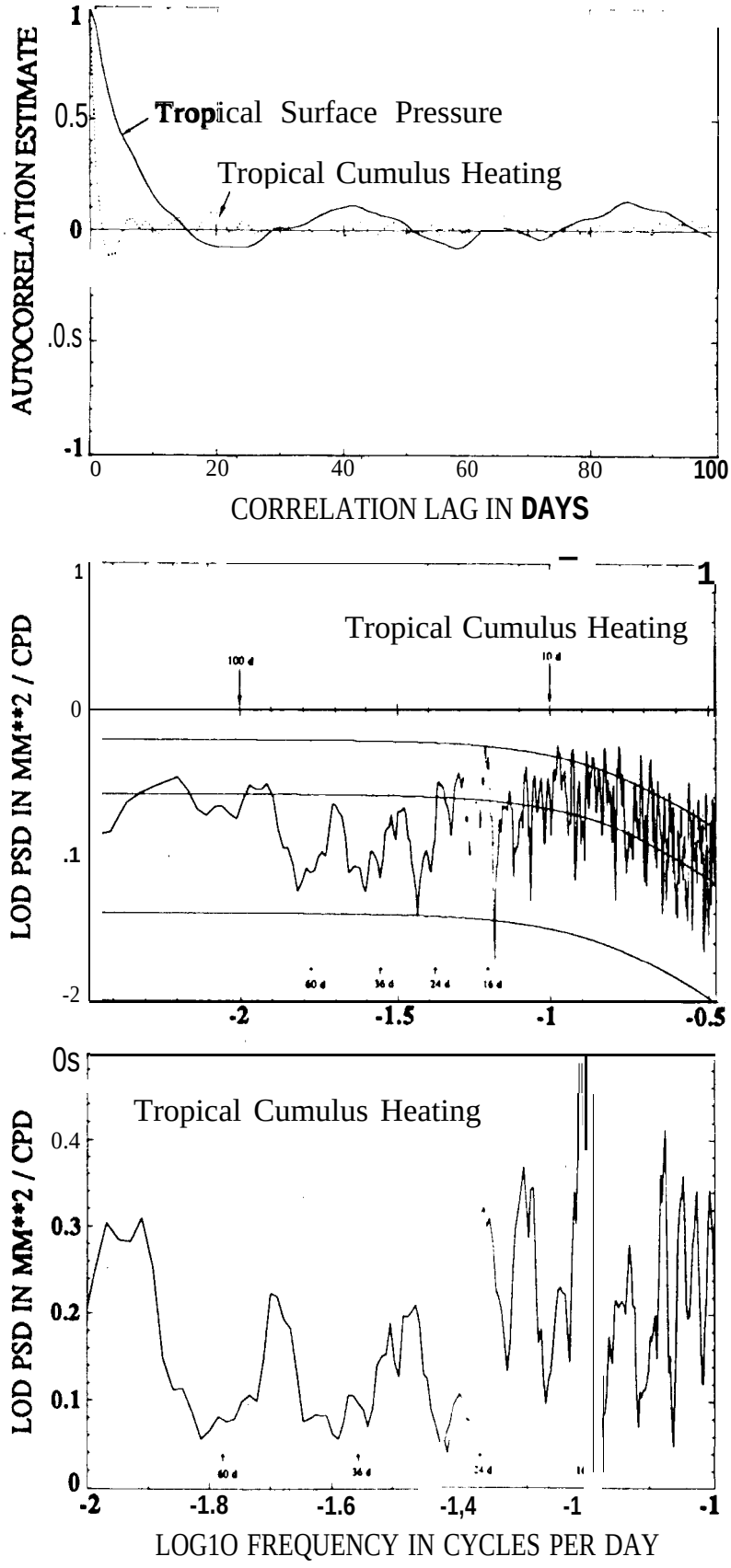
AUTOCORRELATION ESTIMATE
1
0.5
0
.0.S
-1
0
20
40
60
80
100
Tropical Surface Pressure
Tropical Cumulus Heating
CORRELATION LAG IN DAYS
(a)
LOD PSD IN MM**2 / CPD
1
0
.1
-2
-2
-1.5
-1
-0.5
Tropical Cumulus Heating
(b)
LOD PSD IN MM**2 / CPD
0s
0.4
0.3
0.2
0.1
0
-2
-1.8
-1.6
-1,4
-1
-1
Tropical Cumulus Heating
(c)
LOG1O FREQUENCY IN CYCLES PER DAY

Fig. 16